UNIVERSITY OF SOUTHAMPTON

FACULTY OF ENGINEERING, SCIENCE & MATHEMATICS

School of chemistry

A NEW NANOSTRUCTURED SUBSTRATE FOR SURFACE ENHANCED RAMAN SPECTROSCOPY.

By Suzanne Pelfrey

Thesis submitted for the Degree of Master of Philosophy

November 2004

UNIVERSITY OF SOUTHAMPTON

ABSTRACT

FACULTY OF ENGINEERING, SCIENCE & MATHEMATICS
SCHOOL OF CHEMISTRY

Master of Philosophy

A NEW NANOSTRUCTURED SUBSTRATE FOR SURFACE ENHANCED RAMAN SPECTROSCOPY.

By Suzanne Pelfrey

Surface Enhanced Raman Spectroscopy (SERS) is a very promising analytical technique that was first discovered 30 years ago. The substrate most commonly used, for achieving SERS spectra, are roughened silver or gold electrodes. The metals are roughened through a series of oxidation and reduction cycles using electrochemical cycling. However, these surfaces are very irregular with random peaks and troughs, which lead to very irreproducible SERS spectra. In this project a new nanostructured surface has been produced that consists of regularly aligned nanocavities. They are created by electrodepositing gold around a template of polystyrene spheres that are then removed, leaving the inverse structure. The polystyrene sphere diameter used through the project ranged from 400 nm up to 900 nm, corresponding to the visible region of light. It was found that templates based on a 600 nm sphere diameter produced the largest SERS enhancement; the reason for this is believed to be a combination of surface plasmons and confined plasmons leading to an enhanced signal. The 600 nm sample gave rise to excellent SERS spectra using both the 633 nm HeNe and 785 nm diode lasers; however the signal from the 785 nm spectra were of greater intensity. The enhancement factors observed from the nanostructures in this project are factors of 10^2 larger than those observed from roughened gold. In addition the enhancement is reproducible across the sample. The results from this project imply that the surfaces could be tuned to a specific laser wavelength using different sphere sizes and film heights.

Acknowledgements

I would like to thank many people for all of their help over the last year. Firstly, my supervisor Prof. Phil Bartlett, who has given me so many ideas and support throughout the year. I would also like to thank my advisor, Dr Andrea Russell, for giving me the opportunity to undertake this project in the first place. Without Andrea and Phil I would not be here and have been given the chance to go on and do a Ph.D.

My gratitude also goes to Dr Mamdouh Abdelsalem, who has taught me so much throughout this project and has given me a lot of support and advice.

Thanks must also go to Prof. Jeremy Baumberg, Steve Coyle and Tim Kelf from the physics department at the University of Southampton, for their help with the optics side of the project.

I would also like to thank the Russell and Bartlett research groups for welcoming me so warmly at the start of the year, and for keeping me sane after spending days in a darkened room!

Finally, I would like to thank Helen Stanford and Renishaw for their help when there were problems with the laser and spectrometer, and for teaching me so much about the equipment.

Table of Contents

Chapter One: Introduction

1.1 Raman Spectroscopy

Raman Spectroscopy is a very promising analytical technique; spectra can be taken from a very small amount of sample in a non-invasive/non-destructive manner. However the Raman effect is weak. In order to produce a stronger signal, Resonance Raman or Surface Enhanced Raman spectroscopy (SERS) may be used. A number of substrates have been developed for SERS. However, the surface structure of most of these substrates is poorly defined, not easily tuned nor reproducible. This has been a problem with SERS since the discovery of the technique in 1974 by Fleischmann *et al*[1]. By producing nanostructured thin metal films this problem can be resolved. The nanostructured films described in this thesis are highly robust, and can be easily tuned to produce good Raman enhancements.

The aims of this project were:

- To produce high quality substrates
- To correlate SERS intensities with optical properties
- To apply the substrates to the investigation of the adsorption of a series of organic molecules.

1.2 The Raman effect

The Raman effect was discovered by, and subsequently named after, Prof. C. V. Raman in 1928[2]. He began a series of experiments studying the scattering of light by transparent media and soon noticed the presence of a weak secondary radiation of altered wavelengths when liquids were used. However this was quickly extended to any transparent substance when a mercury arc lamp was used to illuminate the substrate and a spectrograph was used to analyse the scattered light. Raman also showed that each line of the incident radiation

gave rise to its own modified scattering, and the frequency shifts, the relative intensities, the state of polarisation, and other features of the new lines and bands were independent of the wavelength of the exciting radiation. The new scattering effect was named the Raman effect and the spectrum of the new lines the Raman spectrum.

1.2.1 Basic theory of the Raman effect

The Raman Effect is the result of a double transition involving three stationary levels. The Raman line corresponding to the transition from the initial level (k) to the final level (n) can only appear when there is an intermediate level (r), which can combine with k and n in absorption or emission, see figure 1.01. The intermediate level only needs to be a virtual state as the interaction of the photon with the molecule and the re-emission of the scattered photon occur almost simultaneously. If there is no such state the corresponding transition is forbidden in the Raman effect.

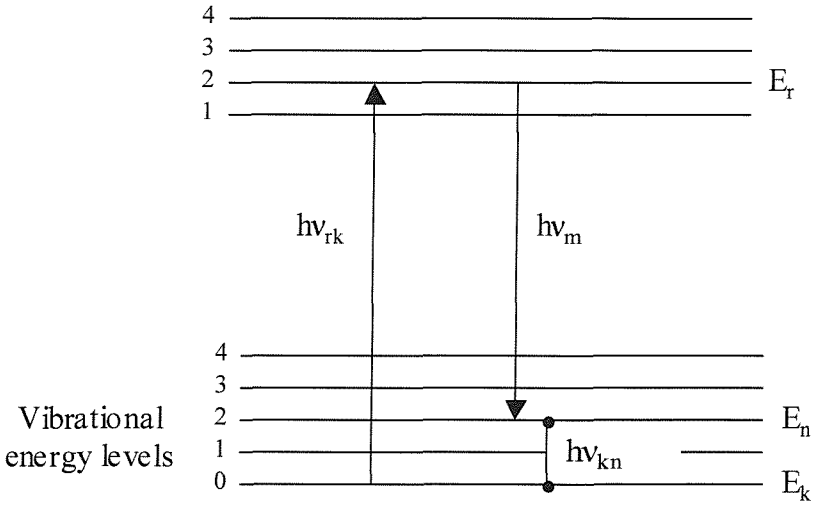

Figure 1.01: Schematic diagram for the theory of Raman Scattering. E_k and E_n are the initial and final vibrational energy levels of a molecule during an interaction with an incident photon. E_r is a virtual state, and the Raman Effect can only occur if this state exists.

The Raman Effect can be described by an elementary classical theory. If a light wave with frequency ν_0 and an electric field strength E is incident on a sample, and E fluctuates at frequency ν_0 then:

$$E = E_0 \cos 2\pi\nu_0 t \qquad (1.01)$$

Where E_0 is the amplitude and t is the time. If a diatomic molecule was irradiated by this wave, a dipole moment μ is induced. μ is given by:

$$\mu = \alpha E = \alpha E_0 \cos 2\pi \nu_0 t \qquad (1.02)$$

Where α is a proportionality constant and is called the polarisability. When the molecule vibrates with frequency ν_1, the nuclear displacement Q is equal to:

$$Q = Q_0 \cos 2\pi \nu_1 t \qquad (1.03)$$

Where Q_0 is the vibrational amplitude. For small amplitudes of vibration, α is a linear function of Q. Therefore:

$$\alpha = \alpha_0 + (\delta\alpha/\delta Q)_0 Q \qquad (1.04)$$

In this instance α is the polarisability at the equilibrium position, and $(\delta\alpha/\delta Q)_0$ is the rate of change of α with respect to the change in a normal coordinate Q also at the equilibrium position. By the combination of these equations the following expression is obtained:

$$\mu = \alpha_0 E_0 \cos 2\pi \nu_0 t + \tfrac{1}{2}(\delta\alpha/\delta Q)_0 Q_0 E_0[\cos\{2\pi(\nu_0+\nu_1)t\} + \cos\{2\pi((\nu_0-\nu_1)t\}] \qquad (1.05)$$

In this expression the first term describes an oscillating dipole, which radiates light at frequency ν_0 *(Rayleigh scattering)*. The second term gives the Raman scattering of frequencies $\nu_0 + \nu_1$ *(Anti-stokes)* and $\nu_0 - \nu_1$ *(Stokes)*.

If the rate of change of α is equal to zero then the second term becomes zero. Therefore the vibration is not Raman active unless the polarisability changes during the vibration.

1.3 Raman/Rayleigh scattering

When an oscillating electric field associated with light interacts with a molecule a small dipole moment is induced through the polarisability of the molecule. This dipole oscillates at the same frequency as the existing light. It is known that an oscillating dipole radiates light at the same frequency at which it oscillates; however this light is not necessarily radiated in the same direction as the existing light, and therefore is scattered. This scattering phenomenon is known as Rayleigh scattering.

The molecules themselves are also vibrating, at frequencies corresponding to normal modes of motion, and these vibrational frequencies can also mix with the exciting light, producing scattered radiation. This radiation, which is detected as shifts from the Rayleigh scattering, is known as Raman scattering. The photons may either be scattered to longer wavelengths, which is known as a Stokes shift, or to shorter wavelengths, which is known as anti-Stokes shift. See figure 1.02.

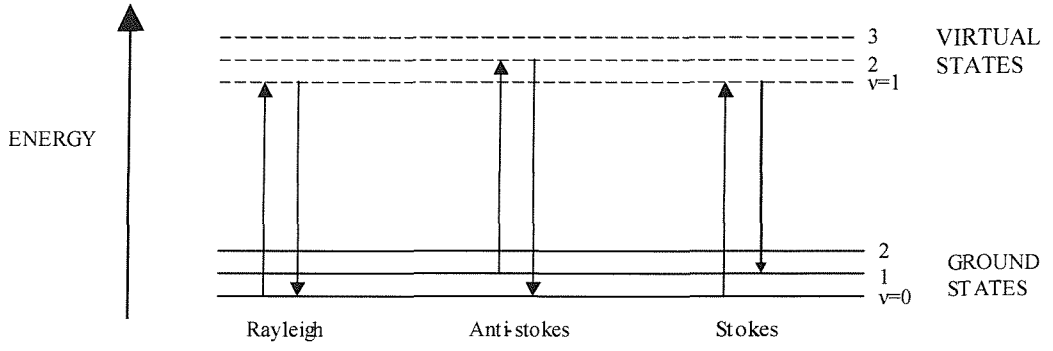

Figure 1.02: Diagram of Stokes, Anti-Stokes and Rayleigh lines.

Only 1 in 10^7 of the incident photons are Raman scattered, and deviations from the incident wavelength are quite small, therefore intense monochromatic incident beams are used (usually lasers). Nevertheless, the Raman signals remain weak. There are two main techniques for increasing the signal obtained: Resonance Raman spectroscopy and Surface Enhanced Raman Spectroscopy, which will be described below.

The main advantage of Raman spectroscopy over other vibrational spectroscopic techniques, such as infrared, is that it is non-invasive and water does not cause interference in Raman, therefore, spectra can be obtained from aqueous solution. Also, glass or quartz cells (rather than NaCl or KBr disks) can be used.

1.4 Resonance Raman Spectroscopy (RRS)

Resonance occurs in Raman spectroscopy when the photon energy of the exciting laser beam is approximately equal to the energy of an electric dipole allowed transition of the material under investigation.

As mentioned previously, when a photon interacts with a molecule a virtual state must exist for Raman scattering to be possible. However, if this state is a real excited energy level of the molecule and the energy of the excitation photon gets close to the transition energy between the two states, then Resonance Raman occurs. This gives an enhancement of the Raman scattering by a factor of up to 10^5. See figure 1.03

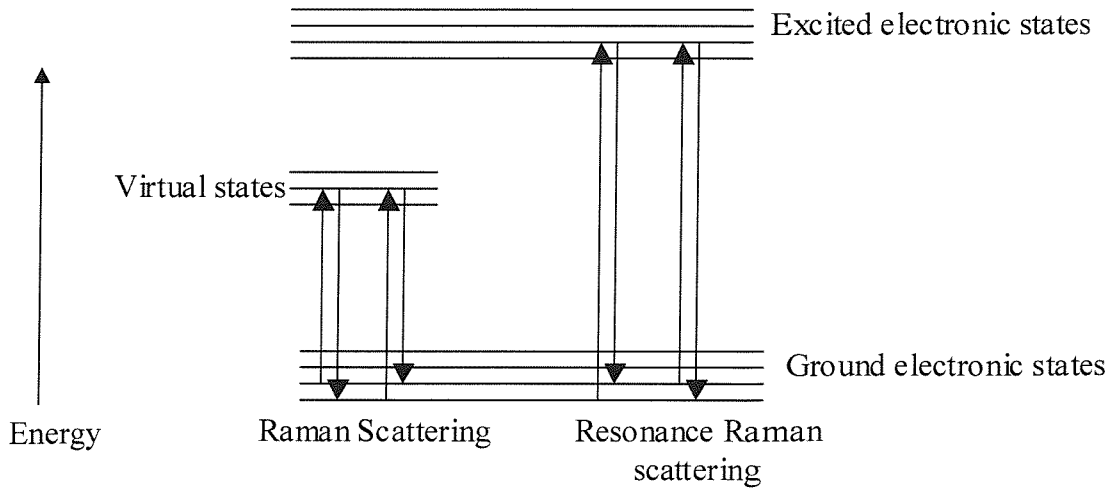

Figure 1.03: Schematic diagram showing Raman and Resonance Raman scattering

1.5 Surface Enhanced Raman Spectroscopy.

Fleischmann[1] first discovered Surface Enhanced Raman Spectroscopy (SERS) in the 1970s, when a roughened silver electrode was used as a substrate for Raman Spectroscopy. The results showed an increase of 10^6 in the Raman signal. Fleischmann attributed this enhancement to the increased surface area of the electrode. However Van Duyne[3] and Creighton[4] both independently showed this to be incorrect. They recognised that the enhancement that could be obtained through roughening an electrode was only a factor of 10. The enhancement that Fleischmann observed was 10^6. Therefore, the field of Surface Enhanced Raman Spectroscopy was born.

1.5.1 Theories of Surface Enhancemed Raman Spectroscopy.

There are two main models employed in connection with the enhancement observed in Surface Enhanced Raman Spectroscopy:

1. Chemical enhancement model – *charge transfer between the metal and the adsorbed molecule.*
2. Electromagnetic theories of enhancement (EM model) – *surface plasmons.*

The Chemical Enhancement model

The chemical enhancement model mainly deals with mechanisms that are specifically related to interactions between the molecule and the metal. Also, the effects of the orientation and the coverage of the adsorbed molecules, metal surface structures and electrode potential are included. The intensity of the signal observed from the chemical enhancement model depends on the charge transfer state mechanism in action, and usually yields enhancements of around $10^2 - 10^4$.

A theory for the chemical transfer of energy has been proposed: a weak interaction between the substrate molecule and the metal surface exists, and the molecular energy level partially overlaps with the conduction band of the metal. Therefore, a charge transfer can

take place. The chemical model predicts that the enhancement is more effective when the surface is rough, as the peaks in the film provide a route for the hot electrons to the adsorbed molecule[5].

The Electromagnetic Enhancement Theory

This model considers the change in the local electric field around the adsorbed molecule, enhancement of the electromagnetic field at the metal surface is caused by the local electric field at the surface.

This model shows that the SERS effect strongly depends on the properties of the metal surface and the frequency dependent dielectric function of the surface metal. The properties of the surface that are of particular importance include the surface shape and size, i.e. surfaces with small irregularly shaped metal particles[6], regularly aligned nanoparticles[7], and inverse structures of colloidal metal particles[8] all show different SERS enhancements.

One mechanism that accounts for the electromagnetic enhancement involves an overlap of the incident radiation wavelength, scattered radiation wavelength, and the surface plasmon resonance wavelength of the substrate.

Surface Plasmon Resonance (SPR)

Surface plasmons are collective oscillations of electrons at the boundary between conductors and insulators, i.e. in this case at the interface between metal and air. Surface plasmon resonance (SPR) is an electron charge density wave phenomenon that arises at the surface of the metallic film when light is reflected off the film under specific conditions. When the SPR is excited at a metal / dielectric interface by a monochromatic light beam, it is observed as a deep minimum in the p-polarised reflected light as the angle of incidence increases. In simple terms it may be thought of as a ray of light bound to a surface, propagating along the surface and presenting itself as an electromagnetic field. The fields

associated with the surface plasmon extend into the media adjacent to the interface and decay exponentially with distance away from the surface.

In order to describe SPR the phenomenon of total internal reflection (TIR) must first be explained. When a light beam propagating in a medium of higher refractive index meets an interface at a lower refractive index at an angle of incidence above a critical angle, the light is totally reflected at the interface and propagates back into the high refractive index medium. Although the fully reflected beam does not lose any net energy across the TIR interface, the light beam leaks an electrical field intensity called an evanescent field wave into the low refractive index medium. The amplitude of this evanescent field wave decreases exponentially with distance from the interface, decaying over a distance of approximately one light wavelength from the surface.

If the TIR interface is coated with a layer of a suitable conducting material (such as a metal) of a suitable thickness the p-polarised component of the evanescent field wave may penetrate the metal layer and excite electromagnetic surface plasmon waves propagating within the conductor surface that is in contact with the low refractive medium. If a non-magnetic metal (i.e. gold) is used, the surface plasmon wave will also be p-polarised and, due to its electromagnetic and surface propagating nature will create an enhanced evanescent wave.

For a plane wave incident beam to excite the surface plasmon on a flat surface both the frequency and parallel momentum must be conserved, however this condition cannot usually be achieved in air or vacuum, and hence, the surface plasmon does not radiate from the surface, but eventually dissipates its energy as heat, producing 'hot spots'.
By roughening the metal surface small particles that have electromagnetic resonances similar to the surface plasmon are introduced. When the particle is small compared to the wavelength of an incident plane wave, a plasmon can be excited that has the symmetry of a time varying dipole. Once excited the dipolar plasmon can radiate.

For surface enhanced Raman spectroscopy it appears to be effective for a system to be able to absorb the photon and localise it. Gratings and flat surfaces adsorb the photon and store

the electromagnetic energy into the surface plasmon, which increases the surface density near the surface. Thereby increasing the electromagnetic energy produced.

When SERS was first discovered it was widely thought that enhancement would result from electromagnetic interactions between a molecule and a flat surface. A popular model, proposed by King, Van Duyne and Schatz[9], attributed the electromagnetic enhancement to the large polarisability when the Raman emitting system is taken to be a composite of the molecule and its conjugate charge in the metal. This model is known as the 'image field model'. This model depends strongly on the distance (r) between the point dipole and the surface. When $r \leq 1.65$ Å, King *et al.*[9] showed that enhancements of 10^6 were possible on a silver surface. However when r was more than 2Å the enhancement dropped to 10^2. Weber and Ford[10, 11] modified the image field model in the early 1980's, by eliminating any point dipole restriction in the theory, this decreased the image field enhancement by a factor of 10^3 for the corresponding values of r. The image field model has now been widely discredited and the majority opinion is that image field enhancement is not an important contributor to SERS[12].

Flat surfaces have been known to produce SERS as above. However it is more beneficial to use rough surfaces to produce SERS spectra, as they produce a greater magnitude of enhancement which has been attributed to the grating effect described above.

Many methods are known for roughening the surface of an electrode: electrochemical roughening through oxidation and reduction cycles in acid, via colloidal deposition or even by the use of gratings. When a surface is roughened using electrochemical cycling, an electrode is put through a series of oxidation and reduction cycles. Fleischmann *et al*[1]. roughened their silver electrode by using a solution of 0.1 mol dm^{-3} KCl, and the electrode was swept from the electrode potential +0.2 V vs. SCE, where AgCl was formed, to –0.3 V where this film was reduced back to silver. However the silver does not redeposit as a smooth film, but rather as clusters which can be up to 200 nm high above the bulk film. By roughening the surface in this manner a film with random peaks and troughs is produced. The peaks will act as 'lightening rods' when an incident light beam is applied to the surface and will draw the electromagnetic beam onto the surface, which in turn will excite the surface plasmons, leading to an enhanced Raman radiation scattering.

However, the rough surfaces that are produced in this manner are not reproducible and, therefore, cannot be tuned to produce the best possible SERS spectra. Ideally substrates for SERS would also be robust, reproducible and easily analysed. Nanostructured films look like a very promising possibility for an alternative SERS substrate.

1.6 Nanostructured Films

Structured metal films are of vast importance for a number of areas of science and technology, for example in fuel cells, gratings and various applications in the field of optics (they can be used to create photonic crystals or photonic mirrors, which exhibit specific, desired optical properties[13-15]). They are also very useful for the study of adsorption, wettability, adhesion and electron transfer mechanisms. There are many different forms of nanostructured films, including: nanodots, gratings, nanocavity or colloidal structures. These structures have become of great interest in the last five years due to the large number of uses mentioned above.

The nanocavity structures are of the most interest for the purpose of this project. The first structure of this type was made by Imhof and Pine[16] in 1997. Velev *et al.*[17] and Braun and Wiltzius[18] also prepared very similar structures shortly afterwards.

1.6.1 Nanocavity structure

The basis of this structure is rather similar to a honeycomb. As shown in figure 1.04 voids are created by assembling polystyrene or silica spheres onto a surface and then filling the voids between the spheres with a metal or polymer. The spheres are then removed leaving voids in their position.

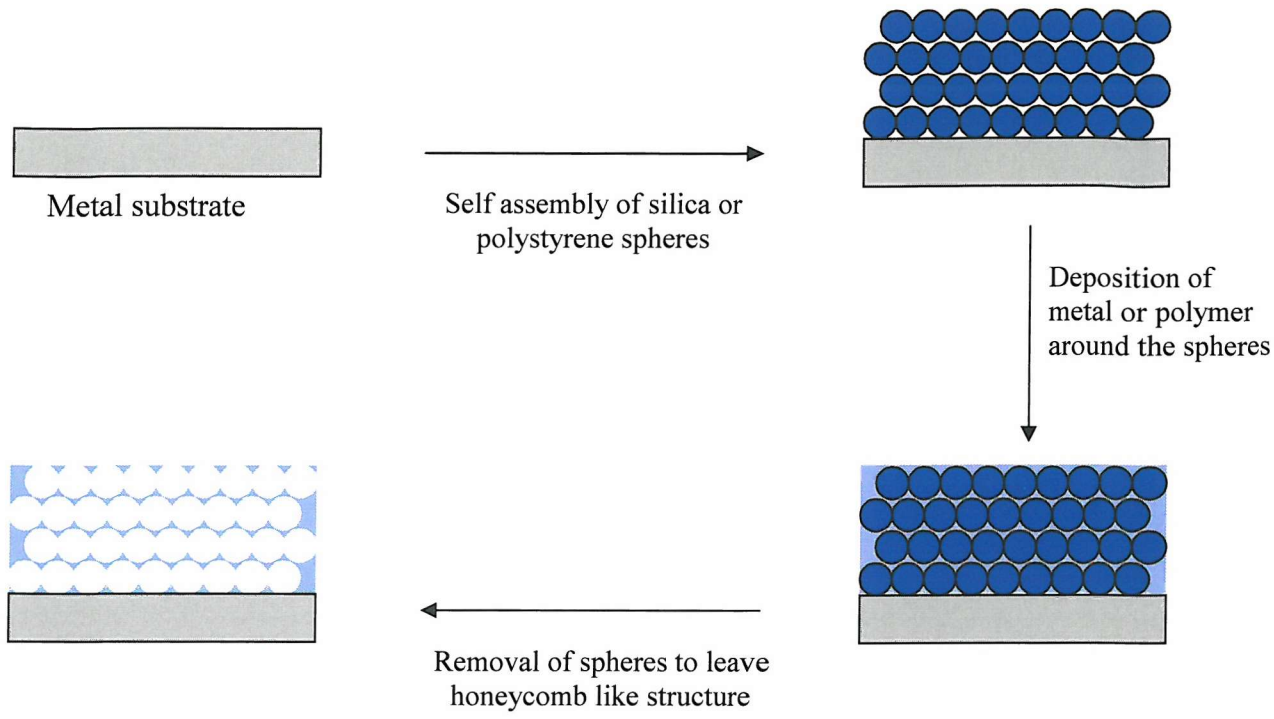

Figure 1.04: Schematic diagram showing a general scheme of how the nanocavity structures are produced.

The original structures made by Imhof and Pine[16] were made in a different manner to that used for the majority of structures made today. They used an emulsion templating procedure, which used an oil-in-formaldehyde emulsion, where the oil droplets acted as the template. The metal surrounded the droplets by the preparation of a metal oxide sol, which was mixed with formamide. The oil containing emulsion was then dispersed into the metal sol, and the droplet size was controlled by centrifugation. Finally the gel was dried and calcinated, leaving the inverse structure. Their method was quite successful and the film looked well ordered, however the technique yielded templates that were irreproducible and lacked absolute control over the pore size.

In contrast, Braun and Wilzius used CdS and CdSe to deposit around polystyrene spheres of 466nm[18]. The spheres were assembled on an indium tin oxide electrode. However their technique for the production of the template uses a sedimentation technique, which produces a multilayer polycrystalline material. These tend to have numerous defects e.g. stacking faults, cracking and grain boundaries.

More recently there have been advances in templating techniques, for example templates can be produced with a monolayer of spheres, and with regular defects[19] and bands[20]. Our group now prepares templates with monolayer coverage and voids are filled using electrodeposition. The main benefits of this technique over methods such as spin coating[21] or electroless deposoition[22] are:

1. Production of a high density material between the voids. The material is deposited in the voids between the spheres as opposed to around the surface of the spheres. This, in turn, means that there will be little or no shrinkage when the spheres are removed.
2. Electrodeposition can be used to prepare a wide range of materials. Both aqueous and non-aqueous solutions can be utilised.
3. Electrodeposition allows control over film thickness, by control of the total charge passed in the cell.
4. The film produced is very smooth, with typical roughness factors that may be fully accounted for by the nanostructure imposed by the spheres.

As mentioned previously these structures are incredibly robust and do not degrade over time and can be reused many times.

1.7 Optical properties of Gold nanostructures

Optical properties of metal films have been of interest since the discovery of the grating effect by Wood in 1902. There have been a number of excellent reviews on this topic in recent years[13, 15], and our group in Southampton has published a very thorough review of the reflectance spectra and optical properties of the nanostructured metal films used in this project[14].

The two main features that are observed from the reflectance spectra from the nanovoid structures are a diffraction pattern and an interference effect when a white light laser is incident on the surface at an angle normal to the surface plane, which will be defined as an incident angle of 0°, as shown in figure 1.05

Diffraction

Diffraction occurs when a ray of light changes course due to the interaction with a substance with a different refractive medium. For example when a ray of light hits water the light is diffracted.

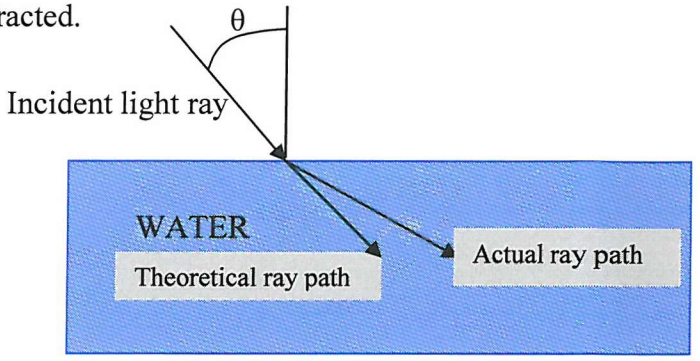

Figure 1.05: Schematic diagram showing an example of diffraction through water, where θ is the angle of incidence

As shown in the above diagram diffraction occurs when light hits a substance of different refractive index, (this also applies to metals). When a beam of white light hits a metal surface, the light is either reflected or diffracted. If the light is diffracted, the energy is either absorbed into the metal, or the surface metal atoms are excited and the photons interact with the excitation wave of the surface metal atoms to create a surface plasmon polariton. These surface plasmon polaritons can dissipate their energy across the surface of the metal leading to hot spots on the surface. The energy of the polariton is released from the surface as a light beam, (shown as the green line in figure 1.06).

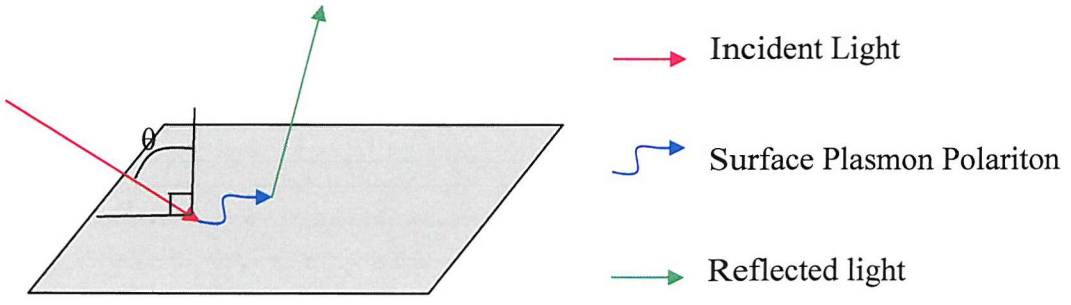

Figure 1.06: Schematic diagram showing light being diffracted as a surface plasmon polariton, where θ is the angle of incidence.

In the case of the nanostructured surfaces used in this project, the surface plasmons can only propagate across the surface when the pores at the surface are small, as shown in figure 1.07.

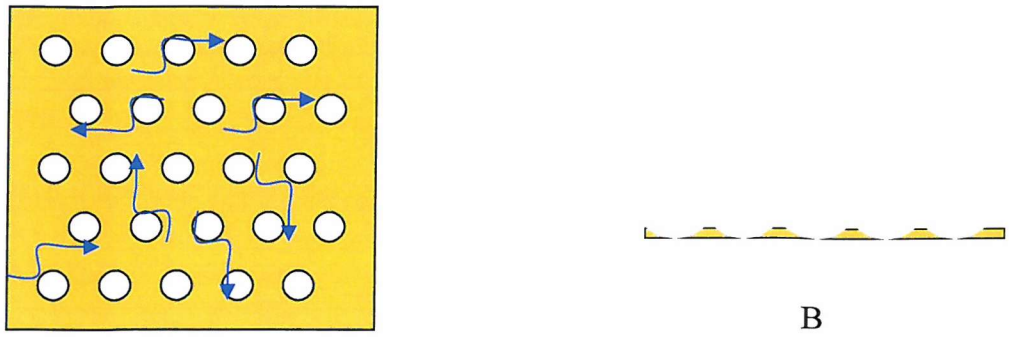

Figure 1.07: Schematic diagram of surface plasmon polaritons propagating between the voids on a nanostructured gold surface (A). Side view of thin film showing the very shallow dishes, and the large area between the spheres (B).

Figure 1.07 shows surface plasmon polaritons moving in between the voids of the spheres. This can only theoretically happen when the distance between the voids is large enough to leave a flat gold surface in between them. As the film increases in height the distance between the pores decreases, until the film height reaches a thickness equal to ½ the sphere diameter, where all the pores are interconnected from the point where the spheres touched in the original template. At this point the plasmons cannot propagate across the surface. i.e.

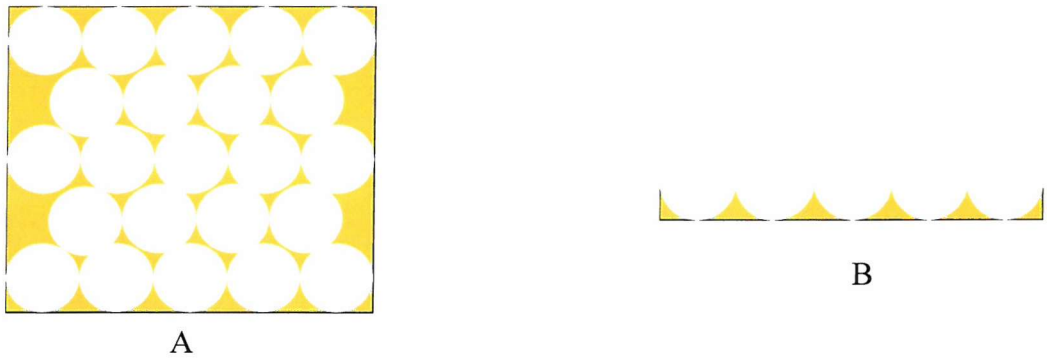

Figure 1.08: Schematic diagram showing a nanostructured gold film at half the height of the original template spheres (A). The area between the spheres has decreased in relation to fig. 1.07. Figure 1.08 (B) shows a side view of a half height film.

The top layer surface area in between the spheres changes as the film height is increased. Figure 1.09, shows two adjacent spheres, with the radius of the sphere marked as r and the distance between the spheres marked as D_s.

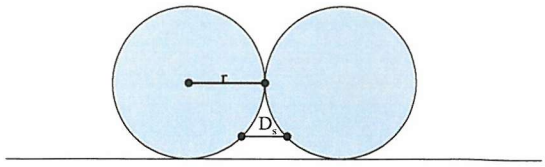

Figure 1.09: Schematic diagram showing the distance in between two spheres and the radius of a sphere.

It can be seen from figure 1.09 that as the radius of the pore increases, the distance between the spheres decreases. As the spheres become closer the area in between the spheres decreases. Figure 1.10, shown below, shows the difference in area between the spheres depending on r at the chosen film height.

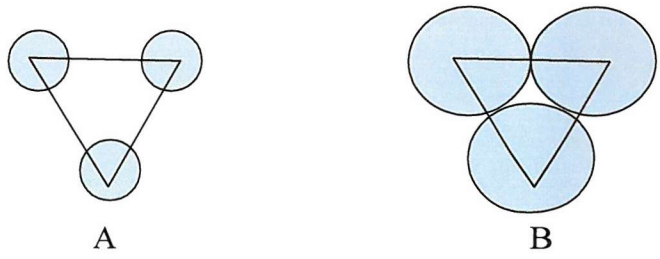

Figure 1.10: Schematic diagram showing the differences in area between the hexagonally close packed spheres. (A) Shows large area between spheres when the radius of the sphere segment at the selected film height is small (as shown in figure 1.07). (B) Shows small area between spheres when they are in contact at half sphere height, as shown on figure 1.08.

Figure 1.10 shows how the surface area of the metal is larger for smaller sphere radii. By comparing figures 1.07 and 1.10, it can be seen that for the propagation of the surface plasmons to occur the film height needs to be less than approximately ¼ of the diameter of the sphere. Alternatively, the film could be greater than ¾ D which would produce the same surface area between the spheres. Therefore diffraction effects occur at thin film and again at thick films.

Interference

When reflectance spectra are taken of the nanostructured gold surfaces the effect of interference occurs at around half sphere height. The voids at this point become spherical enough for the incident light to interact with them, which shows in the reflectance spectra as interference features.

When light interacts with a spherical surface the light can be internally reflected around the pore in a multiple bounce pattern [14]. In principle there could be any number of bounces, however the 1 and 2 bounce models seem to contribute more significantly to the reflection. However the validity of a ray model for cavities of the order of λ is open to question. Figure 1.11 below shows the one and two bounce models for a spherical cavity.

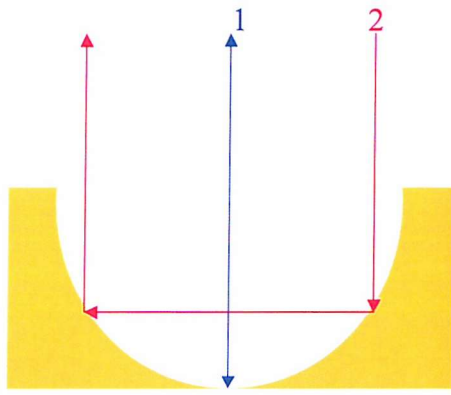

Figure 1.11: Ray paths of an incident plane wave off the spherical void of a gold nanostructure. Showing one bounce and two bounce models.

The interference effect occurs when the incident light interacts with light that has bounced out of the pores. When two waves interact the interference can either be constructive or destructive, as illustrated in figure 1.12, below.

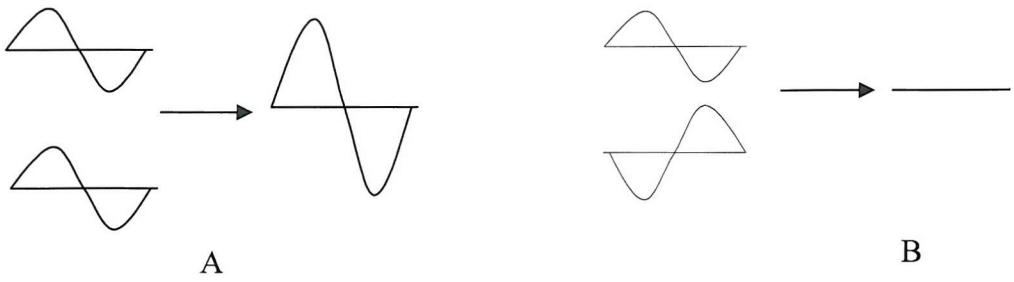

Figure 1.12: Schematic diagram showing the interference of two waves of light, constructive (A) and destructive (B) interference.

This simple theory can be applied to the light being reflected from the pores of the nanostructure. If the light that is reflected from the pore is in the same ray path of another ray of light that has been reflected from the structure then they can interfere either destructively or constructively. This effect is seen in the resulting reflectance spectra from that area of the sample.

As the film height increases to the point that the pores start to close up, the interference effect becomes less pronounced, and as the area between the spheres increases once more, then the plasmon can propagate across the surface again.

A reflectance spectrum of a typical gold nanostructure is shown below in figure 1.13, it shows the different features mentioned above. All spectra were taken using a white light laser at 0° incidence; the spectra are plotted on a log scale and are offset from each other for clarity. From the example spectra shown above it can be seen that the diffraction and interference effects occur between the wavelengths of 500 and 700 nm. The laser predominantly used in this project for the SERS spectra is a 633 nm HeNe laser and therefore, the effects shown above should affect the SERS spectra obtained from these nanostructures. The diffraction of the light and the generation of surface plasmon polaritons are of particular importance because the primary theory of SERS involves surface plasmons, as discussed previously.

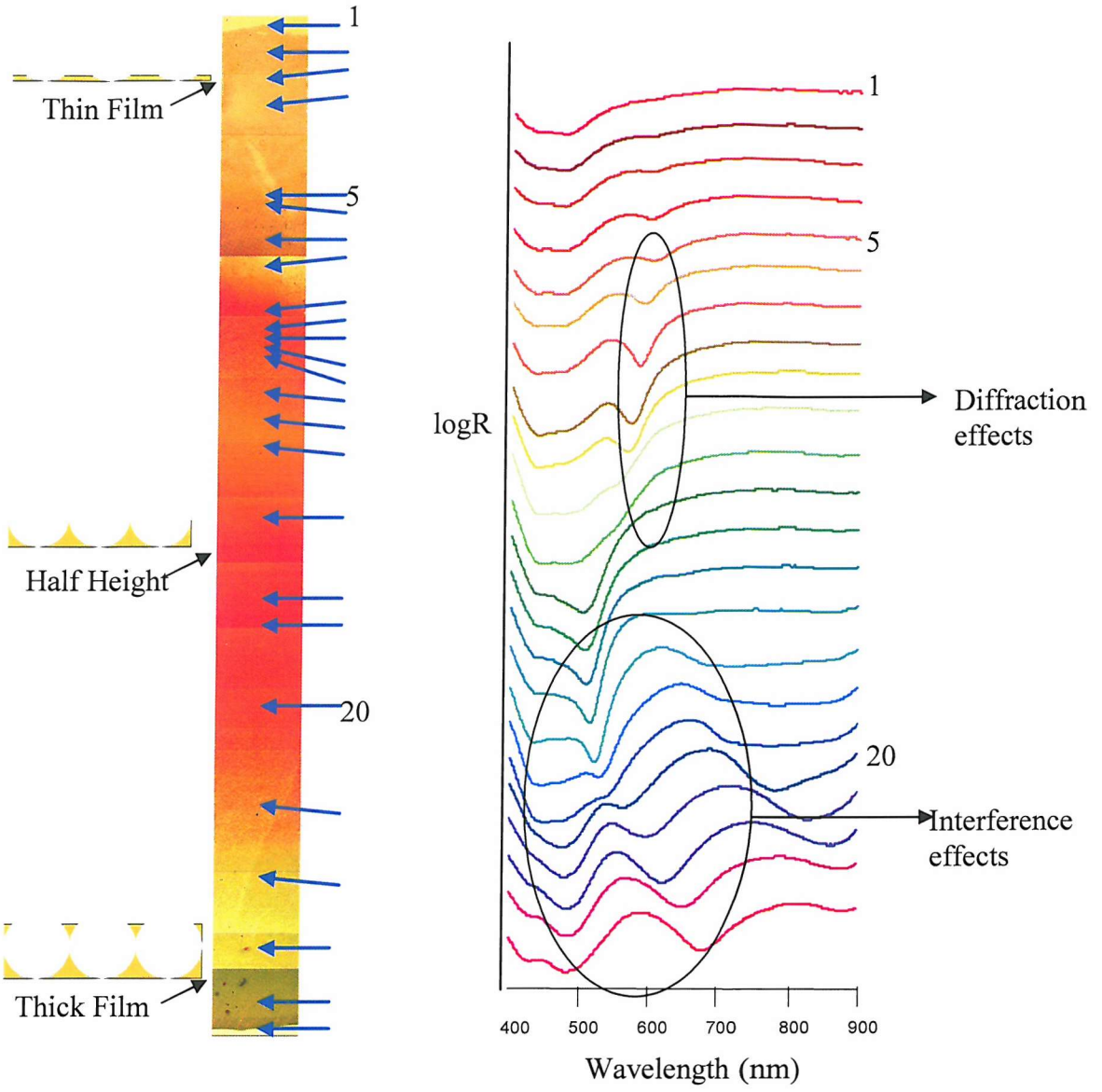

Figure 1.13: Reflectance spectra from a 600 nm gold nanostructure. All spectra were taken using a white light laser at zero incidence. Spectra are plotted on a log scale and have been off set for clarity. The optical images are shown to indicate the change in colour observed as the film height gets thicker. The blue arrows show the points from which a reflectance spectrum was taken.

Chapter Two: Experimental Methods

2.1 Introduction

The experimental work described in this thesis can be divided into five main sections:

- Preparation of the template using thin layer cells.
- Electrochemical deposition of gold through the template.
- Scanning Electron Microscopy.
- Raman spectroscopy (SERS measurements).
- Optical measurements.

2.1.1 Chemicals

The templates were made of monodisperse polystyrene latex spheres (Duke Scientific Corporation) supplied as a 1 wt. % solution in water. The diameters of the spheres used ranged from 350 nm to 895 nm. All solvents used were of reagent grade quality and were used without further purification; isopropanol, tetrahydrofuran (THF), cysteamine, benzenethiol and ethanol were all obtained from Aldrich. The cyanide free gold plating solution (ECF 60 gold plating solution /(10g/l)) was obtained from Metalor Technologies (UK) Ltd. All solutions were freshly prepared using reagent-grade water (18 MΩ cm) from a Whatman RO80 system coupled to a Whatman "still plus" system.

2.2 Preparation of colloidal templates

2.2.1 Preparation of Gold substrates

The evaporated gold electrodes used as substrates were prepared by evaporating 25 nm of chromium, followed by ~250 nm of gold onto a standard sized microscope slide. The substrate was then thoroughly cleaned via ultra-sonication in isopropanol for 90 min, then removed and rinsed with deionised water and dried with a stream of argon (BOC gases).

The substrates were made hydrophilic using a self assembled monolayer (SAM) of cysteamine. Cysteamine was self assembled onto the freshly cleaned evaporated gold electrodes by immersing them into a 10 mmol dm^{-3} ethanolic solution of cysteamine at room temperature for a minimum of three days. The cysteamine layer decreases the contact angle of the water on the gold, which promotes a monolayer of polystyrene spheres to assemble on top of the SAM. There is also a strong electrostatic force between the surface and the negatively charged spheres, encouraging self assembly of the polystyrene spheres.

2.2.2 Assembly of the colloidal template.

The deposition of the colloidal template was carried out using a thin layer cell (~ 2 cm × 1.5 cm) (See figure 2.01) made up of the cysteamine coated gold electrode and a clean, uncoated cover slip (2.2 cm × 2.2 cm) which had been heated in an oven at 100 °C. The electrode and the cover slip were then held 100 μm apart by a spacer cut from Parafilm (Pechiney Plastic Packaging, Inc). The space between the two plates was then filled with the aqueous 1 wt. % suspension of polystyrene spheres.

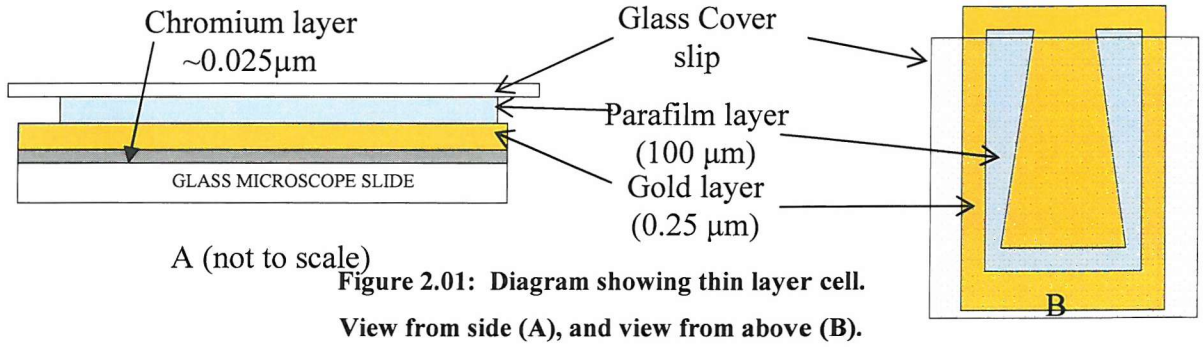

Figure 2.01: Diagram showing thin layer cell. View from side (A), and view from above (B).

The Parafilm is cut into a triangular shape as this promotes a large domain area for the spheres. The filling can be monitored using the transparent cover slip and any air bubbles removed using a very slight argon stream. The thin layer cell was then placed into an incubator at 25 °C (model LMS series 1), which allows control over the evaporation rate, until the template was dry. The glass cover slip and parafilm were then removed before the electrodeposition of gold.

2.3 Electrochemical deposition of gold

Electrochemical deposition was performed using a standard three electrode cell controlled by an Autolab PGSTAT30. The templated gold substrate was the working electrode, a large area platinum gauze was the counter electrode and a home made saturated calomel electrode (SCE) was the reference electrode. The gold films were deposited under potentiostatic conditions at -0.7 V vs. SCE.

The gold plating solution contains an electrolyte of potassium sulphite. The gold ions undergo an efficient two electron reduction at the surface, to produce a smooth layer of gold which was deposited around the polystyrene spheres.

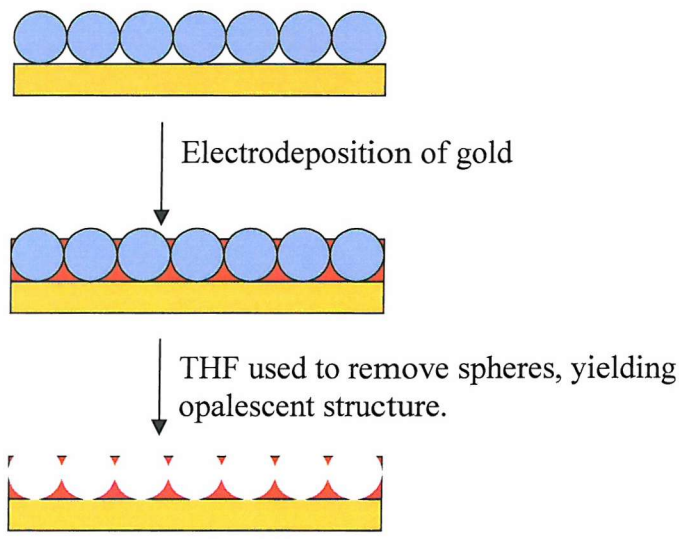

Figure 2.02: Schematic showing the electrodeposition templating process. The gold was deposited around the spheres, yielding a highly robust structure when the spheres are removed.

The samples were then placed in THF for approximately 2 hours to dissolve the polystyrene spheres, yielding the inverse structure as shown in figure 2.02. The film heights on the samples could be varied from very thin film up to one sphere height by raising the sample out of solution using a microstage.

2.4 Scanning Electron Microscopy

The structure and quality of the films were then analysed using an environmental scanning electron microscope (Philips XL30 ESEM). The method of Scanning Electron Microscopy (SEM) was chosen to analyse the templates, because it is a non destructive method which produces images that are easy to interpret by eye. Briefly, electrons are accelerated, by a Tungsten filament source, to energy of 30 keV, the spot size used was 5 keV and images were recorded at magnifications of up to × 20 000.

2.5 Raman Measurements

All Raman spectra were recorded using a 633 nm HeNe laser 'Renishaw 2000 Raman system' (unless otherwise stated). The instrument was calibrated using a silicon wafer, which has a very strong Raman peak at 520 cm^{-1}.

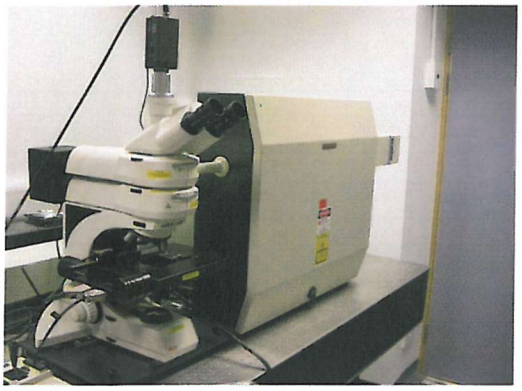

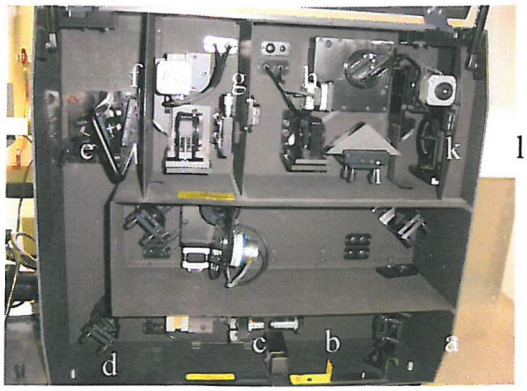

Key:

a) Laser alignment mirror

b) × 40 objective lens and 10 μm pinhole

c) × 4 objective

d) Adjustable mirror

e) Fixed mirror

f) Holographic notch filter

g) Laser filter

h) Spectrographic entrance slit

i) Prism mirror

j) Diffraction grating assembly

k) CCD focusing lens

l) CCD detector

m) Microscope

Laser light

Raman scattering

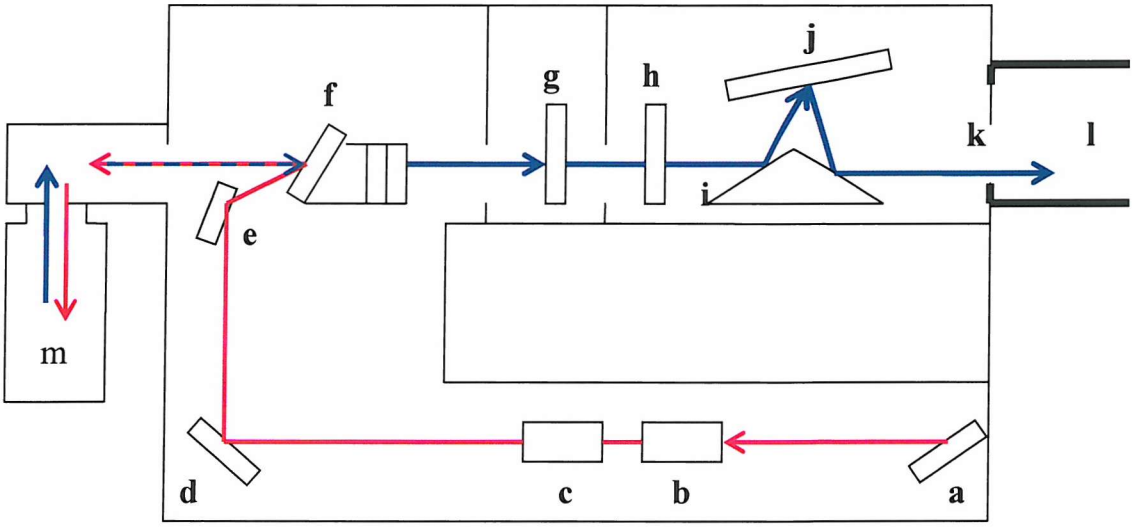

Figure 2.03: The Renishaw 2000 Raman spectrometer. The main components are indicated by the letters a through m.

Figure 2.03 shows a schematic diagram of the Raman spectrometer. As indicated by the red arrow the laser light is directed into the spectrometer from the source laser (RL633 HeNe laser (633 nm) manufactured by Renishaw) onto the laser alignment mirror (a), the light is then directed through the ×40 (b) and ×4 objective (c) lenses. The laser is aligned using the adjustable mirror (d) and reflected onto the fixed mirror (e) and onto the notch filter (f), where it is directed into the microscope and onto the substrate at normal incidence through a × 50 objective, which produces a spot size of 5 μm. The Raman and Rayleigh scattered light and any remaining laser light are then reflected back up to (f) and through to the laser filter (g), indicated by the blue arrow in figure 2.04, where the reflected laser light and Rayleigh scattering are eliminated. The Raman scattering then goes through to the spectrographic slit (h), which was set to 50 μm for all the measurements reported in this thesis. The prism mirror (i) reflects the beam onto the grating assembly (j) and then into the CCD detector (l) through the focusing lens (k). The area of the CCD detector used to capture the Raman scattering is set at 20 x 576 pixels.

The Renishaw 2000 system can perform static or extended scans. A static scan records a spectrum from a narrow range of wavenumbers and the grating assembly remains still, the benefit of this is that spectra can be taken at micro-second intervals. Extended scans require movement of the grating and a spectrum can be recorded over a much broader range of wavenumbers, however the minimum time scale is 10 s for one scan. All spectra in this project were recorded using an extended scan setting with a scan range from 3200 cm^{-1} to 200 cm^{-1}, one accumulation and a scan time of 10 s, the spectral resolution was 2 cm^{-1}.

The system was calibrated using a silicon wafer. The beam was focused onto the silicon through a × 50 objective and was centred using the crosshairs. When the laser spot is defocused it should diverge into concentric rings around the cross hairs, this is achieved by adjusting mirrors (d) and (e) (see figures 5 and 6).

Each sample had spectra taken from each step of the metal film before assembling any adsorbate onto the surface. A solution of 5 mmol benzene thiol in ethanol was used as the adsorbate for all experiments unless specifically stated, the solution was made up with ethanol because water does not wet the inside of the pores of the nanostructure, due to the hydrophic nature of the surface. The thiol was assembled onto the surface by submerging

the sample into the solution for 30 min. Any excess solution was rinsed from the surface using ethanol, and the sample was left to dry for 15 min.

Spectra were taken from each step of each sample using the parameters mentioned above. In some cases spectra were taken at more regular intervals, for example in 100 μm steps down the sample, using an electronic xyz stage to control the distance moved down the sample.

2.6 Optical Measurements

All reflectance spectra were recorded using a BX51 TRF Olympus optical microscope. The samples were illuminated by a white light source and the images were recorded using a CCD camera (DP2 Olympus). A fibre optic coupled spectrometer (Ocean Optics, spectral range 300 – 1000 nm, resolution 1 nm) placed in the focal plane of the image was used to record the spectral response from the selected area, the spot size of the fibre is 50 μm.

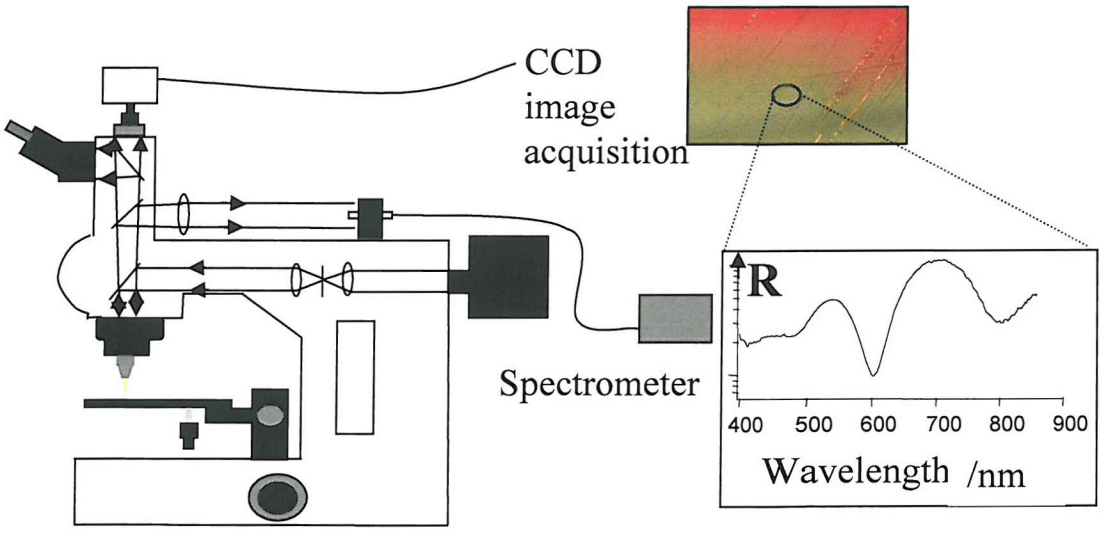

Figure 2.04: Experimental arrangement used to record reflection spectra from small areas of the sample with simultaneous optical microscopy

The same areas of the samples were used for both Raman and Reflectance spectra. Well ordered areas of sample were pin pointed using the SEM images acquired and the optical images were used to find irregularities and defects in the film as reference points. Replicate measurements were made at each step to verify the spectra were a true representation of each step in film thickness.

Chapter Three: Results and discussion

3.1 Introduction

The results of this project can be divided into three main sections:

- Preparation and analysis of gold templates, via Scanning Electron Microscopy (SEM) and optical imaging.
- Surface Enhanced Raman Spectroscopy (SERS) spectra from the gold templates.
- Correlation between the reflectance measurements and SERS spectra.

3.2 Preparation and analysis of gold templates

The templates used for this project were made using a unique technique involving thin layer cells. The procedure for this technique was described in Chapter two. The templates produced are highly robust and reproducible, and various pore sizes and film heights are easily achievable. The quality of the template is excellent due to the high quality of the original crystalline packing of the polystyrene spheres. The packing of the spheres is of excellent quality, because the surface of the evaporated gold is modified by the adsorption of a monolayer of the thiol cysteamine. The layer of cysteamine has two effects:

1. *The contact angle of water on the gold is reduced.*

The contact angle of water on a gold surface was found to be approximately 70° (or 160° for direct comparison to the diagram shown in figure 3.01) meaning that the droplet does not spread on the surface, as shown in figure 3.01. However when the surface is modified by the addition of the thiol the contact angle decreases to approximately 35°.

Figure 3.01: Schematic diagram showing the difference in contact angle of water on (A) evaporated gold, and (B) evaporated gold modified by the addition of a monolayer of cysteamine

The water droplet spreads when the gold has been treated with thiol because cysteamine has an NH_2 group which projects up from the surface. This makes the surface more hydrophilic and the water droplet therefore spreads due to the interaction of the H_2O and NH_2.

2. *The NH_2 group is protonated in water at neutral pH, leading to a positive charge on the surface.*

The polystyrene spheres have a negative charge, so a strong electrostatic interaction occurs between the spheres and the thiol, drawing them closer to the surface. The combination of these two effects contribute to a well packed monolayer of polystyrene spheres self assembling onto the gold surface.

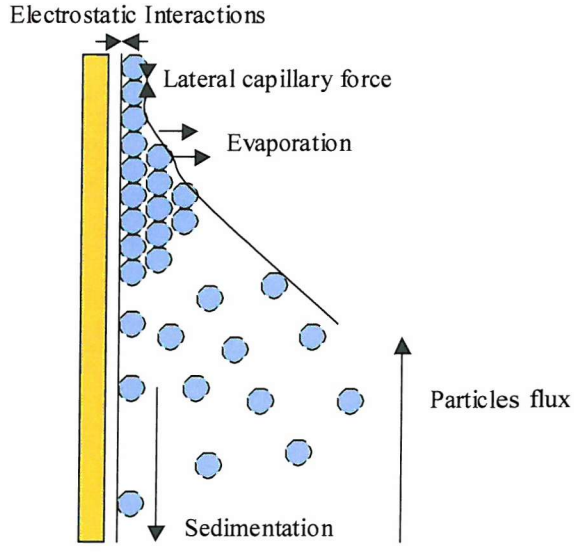

Figure 3.02: Schematic showing the self assembly mechanism of the polystyrene spheres.

As mentioned previously the contact angle of water on the treated gold is approximately 35°, this has an effect on the lateral capillary force. As shown in figure 3.02, the lateral capillary forces between the polystyrene spheres are a dominant factor in creating a monolayer of spheres.

Capillary forces provide interactions between the particles, which are mediated by fluid interfaces [23, 24]. Particles that are suspended in solution attract each other because the liquid meniscus, which exists in between the particles, deforms in such a way that the gravitational potential energy of the two particles decreases when they approach each other. However this gravitational effect does not affect small particles enough to lead to self assembly, as the spheres are too small. However, immersion forces are related to the wetting properties of the surface (discussed above) rather than the size or shape of the particles. An immersion force exists between two particles in solution; two hydrophobic particles would attract each other and essentially bond to each other, which increases their combined vibrational entropy. The combination of the immersion forces and the wettability properties of the substrate result in a monolayer of spheres being produced[25].

When the water has evaporated from the cell and the template has dried, it appears opalescent, with colours ranging from red to green, due to the Bragg diffraction of light from the spheres[26]. The colours are clearly visible when illuminated from above with white light. Figure 3.03 shows an array of 700 nm spheres that are hexagonally close packed.

A B

Figure 3.03: Scanning Electron Microscope images of monolayers of 700 nm polystyrene spheres, on an evaporated gold substrate treated with thiol. Figure 3A shows the hexagonal close packed order of the sample, and figure 3B shows the edge of the same sample as viewed from an angle of 30°.

The close packed structures (such as that shown in figure 3.03) were then used as templates for the electrodeposition of gold, as discussed in chapter 2. They lead to very well ordered nanostructured gold films, which were then used for SERS.

3.3 Surface Enhanced Raman Spectroscopy (SERS) on gold nanostructures.

3.3.1 Surface properties of the Nanostructured Gold

Roughness

In order to show that it is the nanostructure giving the enhancement observed and that the structure is not rough, the surface area can be measured electrochemically. By performing an acid cyclic voltammogram (CV) the area of the electrode can be measured from the oxide reduction peak in the CV. It is known that 386 μC of charge corresponds to a surface area of 1 cm^2 on gold. [27, 28]. The charge in coulombs can be calculated by dividing the area of the reduction peak, which would be in units of V A, by the scan rate, which is in units of V s^{-1}.

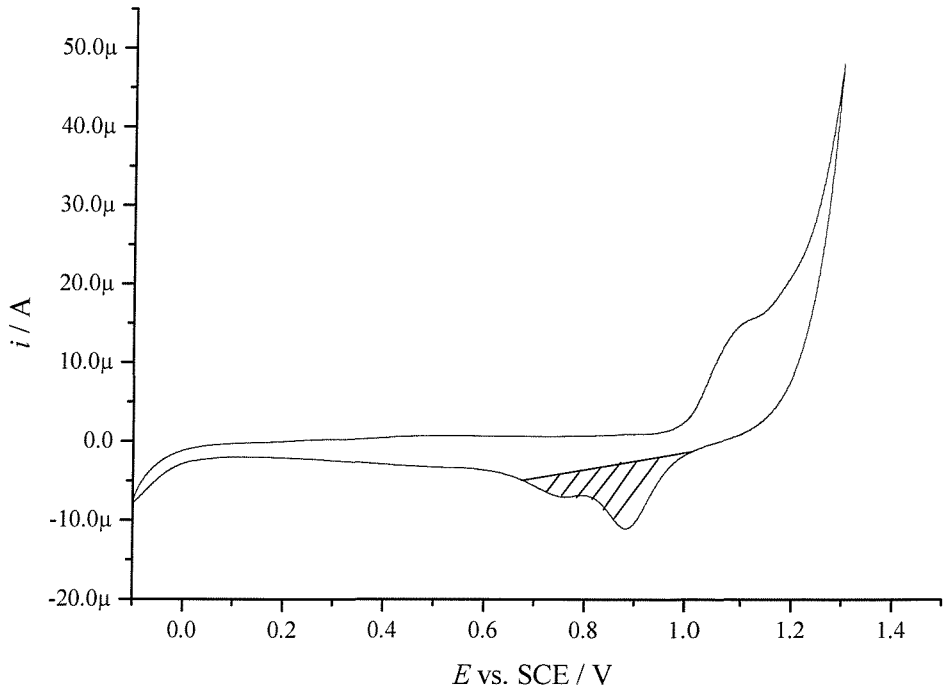

Figure 3.04: Cyclic voltammogram of a nanostructured gold electrode, in 50 mM H_2SO_4. Potential scanned from –0.1 to 1.5 V vs. SCE . Scan rate of 100 mV s^{-1}. The nanostructure was made from a 600 nm sphere size template with a film height of 300 nm (½ sphere diameter)

Figure 3.04 shows a CV of nanostructured gold film that was made from a 600 nm sphere size template, a film of 300 nm in height was electroplated around the spheres. The template was then removed by dissolving the polystyrene spheres in THF while sonnicating the sample for 30 min. The area of the electrode was defined by varnishing around the structure to give an approximate area of 0.044 cm^2.

The area shaded on the CV above was used to calculate the charge passed.
Area of reduction peak was found to be 2.79 x10^{-6} VA. The scan rate was 100 mV s^{-1}. Therefore by dividing the area of the reduction peak by the scan rate a charge of 2.79 x 10^{-5} C was found. 386 μC gives a surface area of 1 cm^2[27, 28]. Therefore, the surface area of nanostructured gold was 0.072 cm^2. The area of the electrode was measured as 0.044 cm^2. Therefore the surface area of the electrode has increased by a factor of 1.6. This value is in comparison to 3.5 for the roughened gold surfaces that are normally used for SERS[4].

Figure 3.05 shows the CV for flat gold overlaid by the CV for nanostructured gold. Each CV was divided by the geometric area of the electrode, to allow a direct comparison in the reduction/oxide stripping peak.

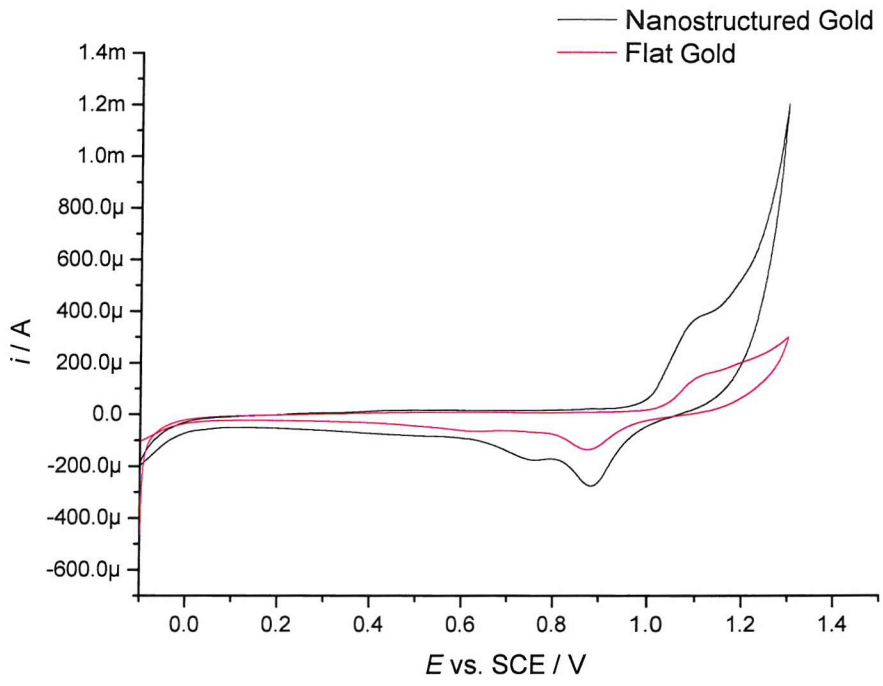

Figure 3.05 Cyclic Voltammogram of a nanostructured gold electrode and an evaporated gold electrode, vs SCE in 50 mMol H_2SO_4. Potential scanned from –0.1 to 1.5 vs SCE / V. Scan rate of 100 mVs^{-1}. The nanostructure was made from a 600 nm sphere size template with a film height of 300 nm (½*D*).

This figure shows that the reduction peak for the nanostructured film has increased in area in relation to the flat gold. As stated previously, the roughness scale factor of the nanostructured gold is 1.6, which means that the surface area has been increased by a factor of 1.6. The surface area has increased due to the spherical cavities of the structure. However, the increase in surface area is only a small fraction of that of the roughened electrodes commonly used in SERS. Therefore this implies that the structure is the cause of any enhancement observed in this project rather than the roughenss.

Robustness

The structures are highly robust and reusable, they do not degrade over time or produce an oxide layer when in contact with air. The main advantage of these structures is, once a

chemical has been adsorbed onto the surface, such as benzene thiol, is that spectra can be taken and then the benzene thiol can be stripped from the surface without incurring any damage to the substrate. The Au-S bond is broken by electrochemically cycling in 10 mM H_2SO_4, from –0.4 to 0.4 V vs. SCE, repeated up to 20 cycles. Figure 3.06 shows the first and last cyclic voltammogram of a 600 nm gold structure that was treated with benzene thiol. The two different CVs show clearly that the thiol has been stripped as the final cycle produces a CV that is expected for gold in acid.

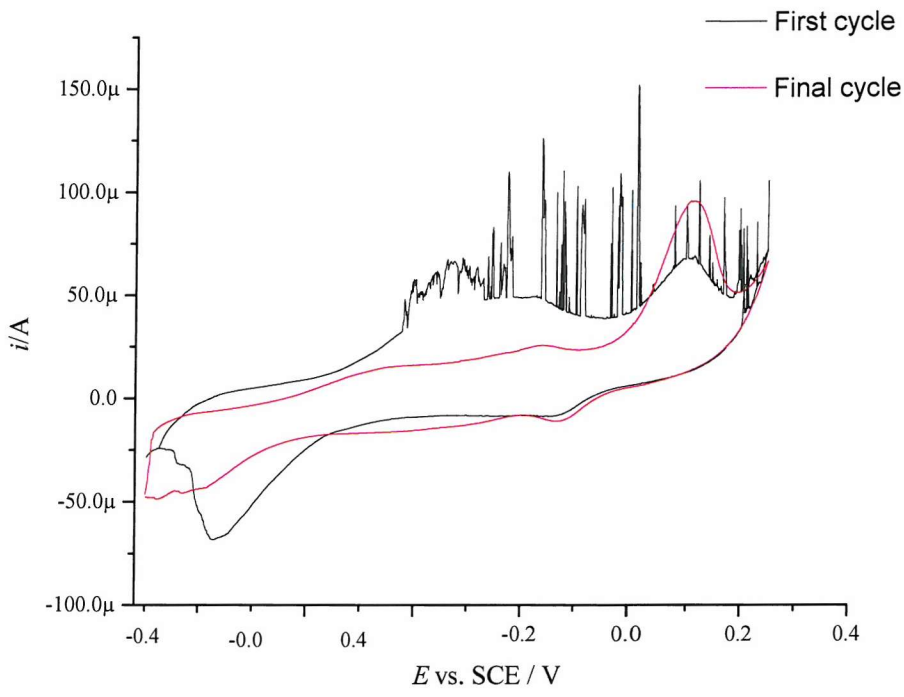

Figure 3.06: Cyclic Voltammogram showing a nanostructured gold electrode, which was made from a template of 600 nm spheres. The layer of thiol was stripped from the surface using 10mM H_2SO_4, the potential was swept from –0.4 to 0.4 V vs. SCE, repeated for 20 cycles. The blank line shows the first cycle, with contaminants on the surface. The red line shows the final cycle of the clean gold.

The first cycle shows that the gold surface is covered with thiol and other contaminates. The final cycle is that of clean gold, as expected for gold in acid. Once the substrate has been stripped of thiol it can then be reused.

3.3.2 Benzene Thiol.

For the SERS analysis of the nanostructures in this project, benzene thiol was chosen as the adsorbate. Benzene thiol bonds strongly to the gold surface, through a Au – S bond. The benzene ring is held away from the surface where it can bend and stretch freely. The Benzene ring stretch produces an unmistakeable peak at 1571 cm^{-1}, which dominates the spectra for the thiol. This peak has been chosen for analysis of spectral intensity and enhancement measurements, in this project.

A SERS Spectrum of benzene thiol is shown below in figure 3.07.

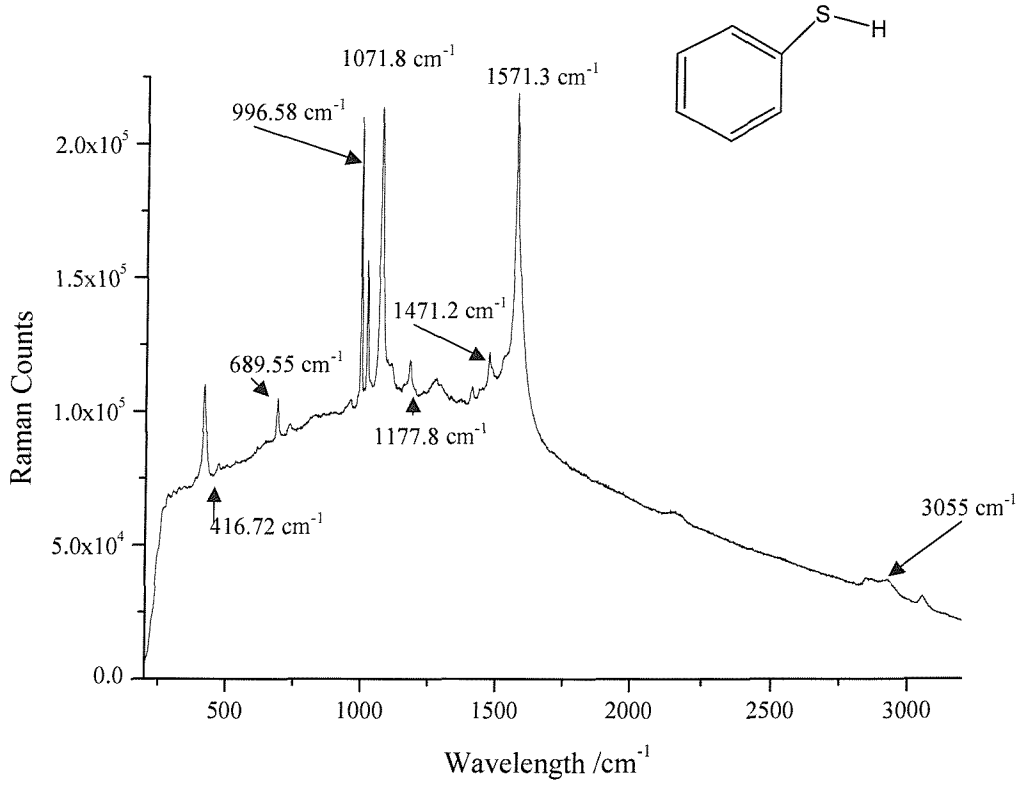

Figure 3.07: Surface Enhanced Raman Spectrum of benzene thiol adsorbed onto a nanostructured gold surface, produced by the hexagonal close packing of 600 nm polystyrene spheres, which act as a template for electrodeposition of gold into the voids left by the spheres. Spheres then removed by dissolving in THF, to produce a nanostructured surface. The Spectrum was taken using an extended scan range of 3200 to 200 cm^{-1}, an accumulation time of 10 s and 1 accumulation. The spectrum was acquired using a 633 nm HeNe laser at 3 mW, with the Renishaw 2000 system, the spot size of the laser was 5 µm.

The spectrum above in figure 3.07 shows very strong peaks, the assignments of which are given in Table 1 below. There is a cut off at 200 cm^{-1}, which is due to the interference of the notch filters of the spectrometer when the reflected Rayleigh and Raman scattering are separated.

Assignment of the spectrum was made with reference to Sang Woo Han, *et al.* [29] and Nam Hoon Kim, *et al.* [6]

Table 1: Peak assignment for the SERS spectrum of benzene thiol, as shown above in figure 3.07

SERS Peak (cm^{-1})	Assignment
3055	a_1, ν(C–H)
1571	a_1, ν(C–C-C)
1471	a_1, ν(C–C)
1177	a_1, β(C–H)
1071	a_1, β(C–C–C) & ν(C–S)
1020	a_1, β(C–H)
996	a_1, β(C–C–C)
689	a_1, β(C–C–C) & ν(C–S)
416	a_1, β(C–C–C) & ν(C–S)

The spectra obtained throughout the project closely resemble that of published SERS spectra of benzene thiol in terms of position and relative intensity of bands[6, 29].

As mentioned above, the strongest peak in the spectrum is the benzene ring stretch seen at 1571 cm^{-1}, it is this peak that has been used to show relative intensities of different spectra. The Peak was measured from the top to the baseline for each spectrum as illustrated in figure 3.08.

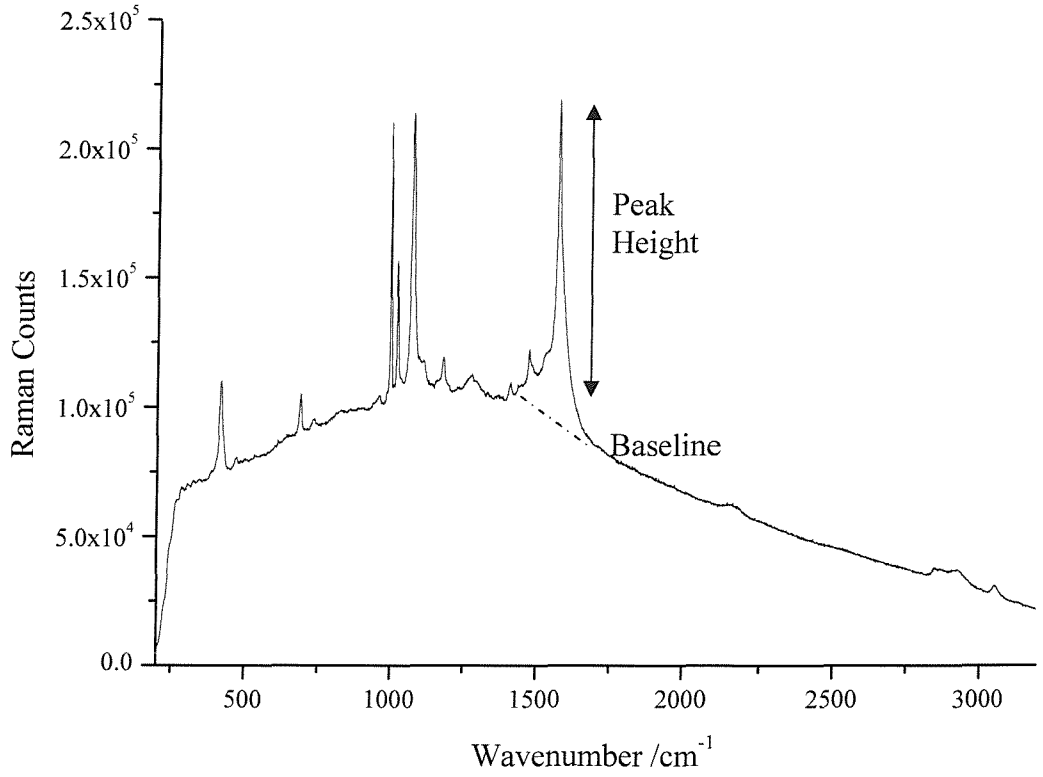

Figure 3.08: Shows a spectrum of benzene thiol on nanostructured gold, the peak height of the 1571 cm^{-1} band was measured from the tip of the peak to the baseline, indicated by a dotted line.

There were a number of different variables to test in order to find the best possible structure for achieving good SERS spectra, including the sphere size of the initial template, the film height of the structure, laser power and laser wavelength. The sphere size variable was investigated by making templates with the sphere sizes ranging from 350 to 895 nm in diameter.

3.3.3 Sphere size dependence

Each sample was prepared in a similar manner, with the templates prepared using a thin layer cell, as described previously. Gold was electroplated into the voids of the spheres, where the film height was controlled by the charge passed, using the Faraday law. Given that the film height can be controlled electrochemically, the film can be grown in steps. The charge can be set to deposit, for example, 50 nm and then stop. The sample can then

be raised out of solution, and another 50 nm deposited etc. until the film is at the height of one sphere diameter (1*D*). The typical films obtained are shown in figure 3.09:

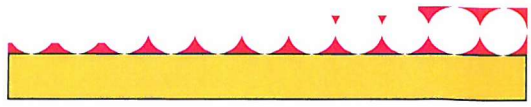

Figure 3.09: Schematic diagram showing a typical graded nanostructured gold film.

For clarity, the overall height of the film around the spheres will be referred to as the film height, with the height each individual step within the film height being called the step height. The distance that the sample was raised out of the solution, to create the step, will be referred to as the step width, shown in figure 3.10

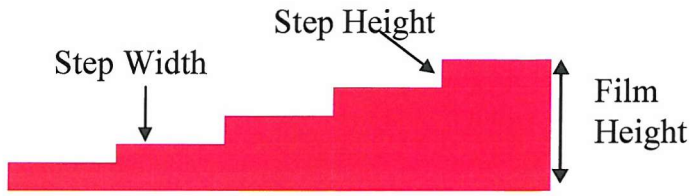

Figure 3.10: Diagram showing the difference between film height, step height and step width of the deposited gold film.

If the film height is graded on each sample then it is possible to locate a film height for each sphere size that gives a good SERS spectrum. The samples made are summarised in table 2.

Table 2: Details of gold samples used to test sphere size dependence of the nanostructure for the purpose of giving good SERS spectra. The table shows the size of sphere used, the number of electrodeposited steps on each sample and the height of each step.

Sphere size (nm)	Number of electrodeposited steps	Calculated Step Height (nm)
450	4	100
500	5	100
600	5	120
700	7	100
800	8	100
895	4	200

Each sample was tested for a Raman signal by adsorbing benzene thiol onto the surface. Three spectra were taken at each step on the sample and the peak height at 1571 cm^{-1} was measured for each spectra, and an average was determined. The results are summarised in figure 3.11.

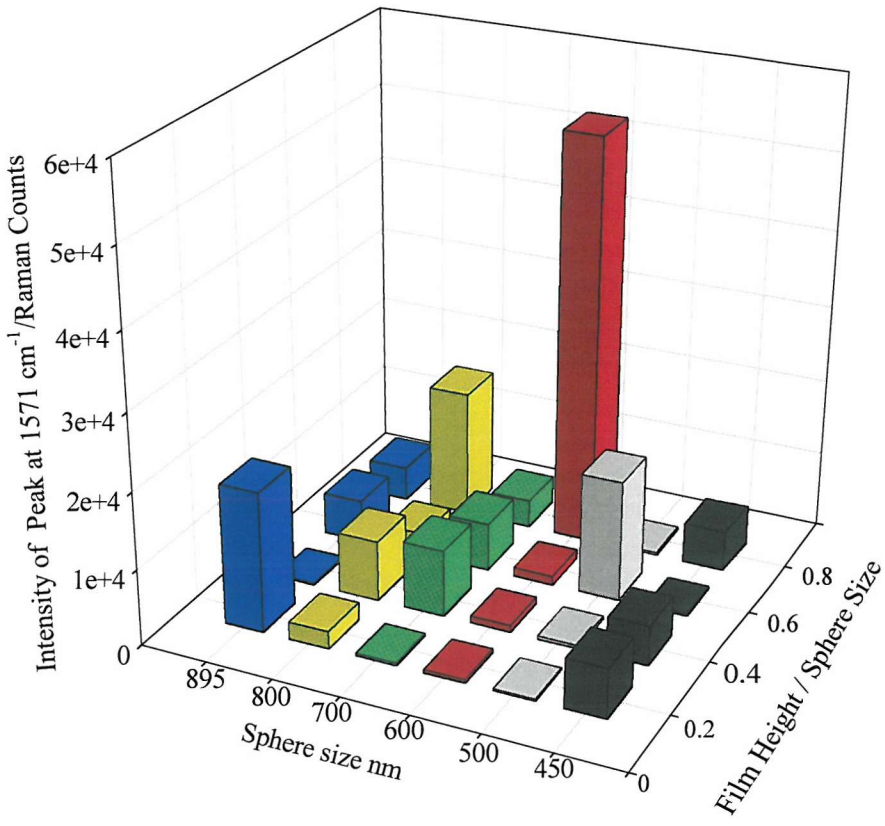

Figure 3.11: The peak intensity of the 1571 cm^{-1} Raman band, of each different sphere size structure, sizes are 450, 500, 600, 700, 800 and 895 nm spheres as a function of film height. Spectra were taken from each step of each sample, and the results were averaged and summarised above. Spectra were collected using a 633 nm HeNe laser at 3 mW power. The scan range was 3200 cm^{-1} to 200 cm^{-1}. The accumulation time was 10 s and 1 accumulation was taken.

The most obvious feature from figure 3.11 is the very large peak intensity for the 600 nm sample. The intensity from the ¾ *D* and above area of this sample shows an intensity of over three times that of any area of any other sample. Another interesting point is that the sphere sizes that are closest to the wavelength of the laser (633 nm), namely 500, 600 and 700 nm, show very little enhancement of the signal below a film height of ½ *D*. The 450, 800 and 895 nm samples show a more general enhancement across the samples, with no area showing an enhancement of more than two fold more than any other area. For example the 450 nm sample shows a height of around $1x10^4$ Raman counts, for the whole

sample. The 895 nm sample shows the largest peak height for the first step, which is interesting, as this is the sphere size that has the largest deviation from the wavelength, implying that it may interact with the laser light differently to the other sphere sizes.

The main observation to be made from the data for the sphere size dependence was that 600 nm spheres produced the greatest enhancement for benzene thiol, at a wavelength of 633 nm (i.e. using a HeNe laser). Therefore to further investigate the variable of film height, the 600 nm templates were used to produce the structures.

3.3.4 Film Height Dependence

Thin Films

From the discussion previously in section 1.7 regarding the optical properties of these structures, there are different modes of the plasmon polariton in the reflectance spectra as the film height increases. Therefore it is expected that the manner in which these modes of the plasmon affect the Raman enhancement may be observed by changing the film height in a more gradual way.

The film height can be varied either by draining the plating solution from the electrochemical cell, or the electrode can be raised out of the solution, while the plating process takes place. However these methods do not allow control over the film height obtained, therefore films with 500 μm step widths were made by raising the sample out of solution using a microstage.

Thin nanostructured films were originally thought quite promising as SERS substrates due to the surface plasmon mode observed in the reflection spectra at films below 0.2 sphere height ($^1/_5D$). This mode is due to the diffraction of light, which is caused by a six fold grating effect, which corresponds to the long range order of the crystal structure, as shown in figure 3.12

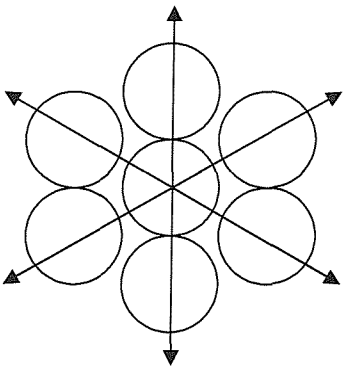

Figure 3.12: Schematic diagram showing the directions of grating effect that can be seen from the assembled hexagonally close packed nano-void structure.

However the 600 nm sample, shown in figure 3.11, displayed very little enhancement in this area, therefore a more graded sample was prepared to see if any enhancement can be obtained from a thin film. The sample prepared was a well ordered 600 nm template, which had a film height graded from 0 to 150 nm (¼*D*). Steps were prepared with 500 μm step widths down the sample and there were nine steps in total. The reflectance spectrum and the SERS spectra of the thin gold film 600 nm sample are shown in figure 3.13:

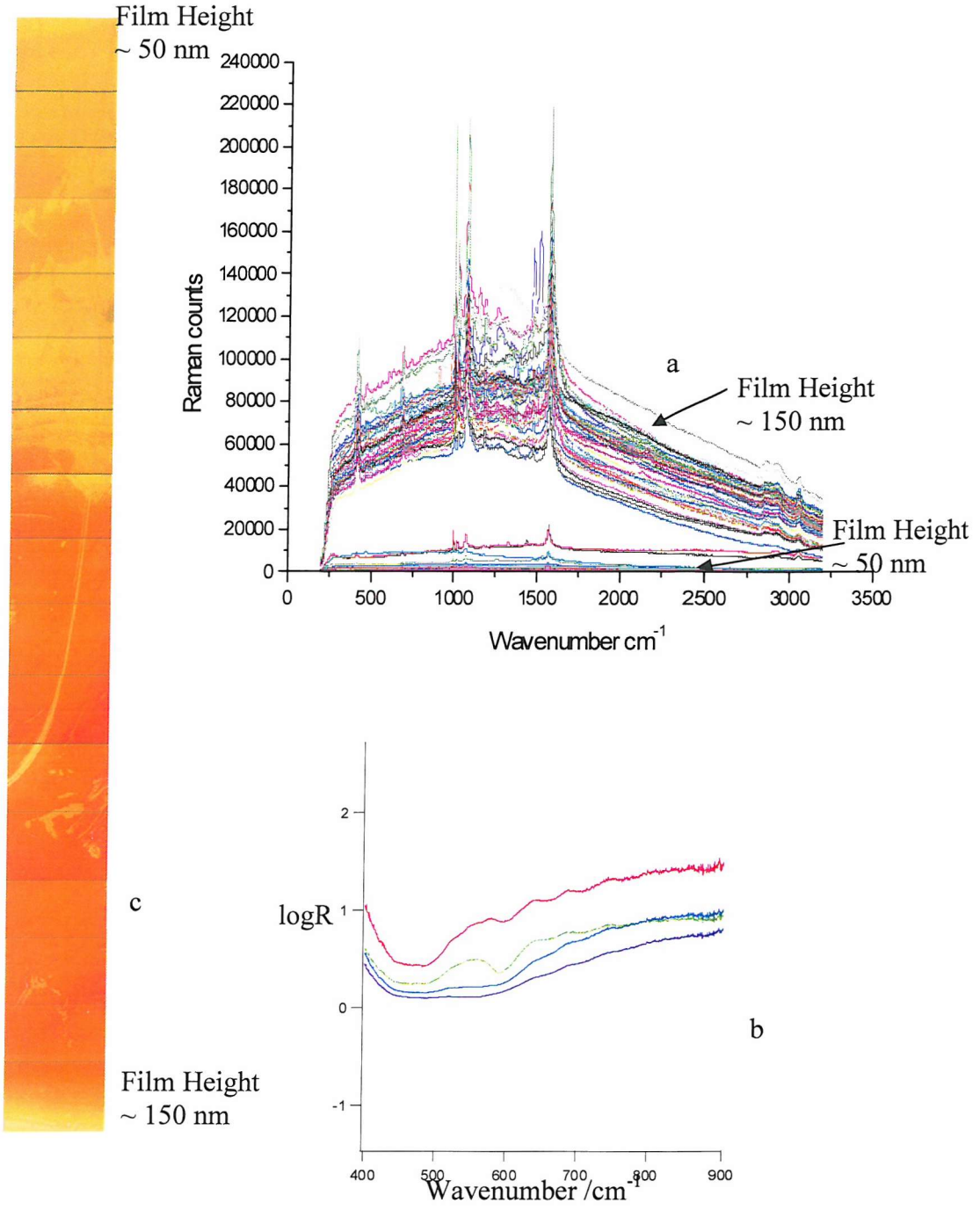

Figure 3.13: SERS (a) and reflection (b) spectra for a gold 600 nm sample with a graded film height up to 150 nm, with the optical images (c) of the film. One spectrum was taken every 100 µm down the sample. Each spectrum was taken using an extended scan range from 3200 to 200 cm^{-1}, with a 633 nm HeNe laser at 3 mW power. An accumulation time of 10 s and 1 accumulation

The reflectance spectra for the thin film 600 nm shows a diffraction pattern from the surface plasmons which are propagating in between the voids of the sample. It is more

likely that the dip in reflectivity comes from the diffraction of the light rather than any interference as the film is not thick enough for the pores to reflect light within themselves.

The SERS spectra in figure 3.13 show two areas of enhancement, the spectra that are 20,000 counts and below arise from an area of the thinnest film. When the film height approaches 100 nm the signal is significantly stronger and the difference is clearly visible in the spectra above. Given the number of spectra taken it is not easy to see where on the sample the best spectrum was obtained. Therefore the same results are shown in figure 3.14 as a function of film height in map form:

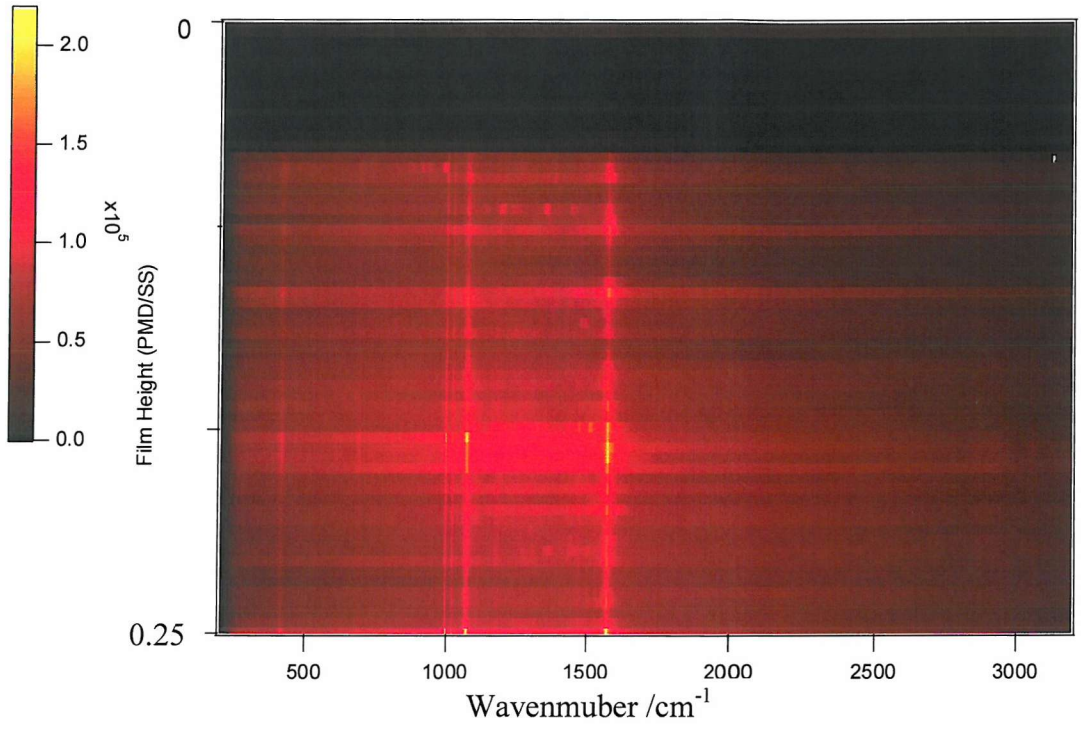

Figure 3.14: SERS spectra of benzene thiol on 600 nm gold sample with film height up to 150 nm. Spectra plotted as a function of film height/sphere size as a map form. Each spectrum was taken using an extended scan from 3200 to 200 cm^{-1} using a HeNe laser at 3 mW power. Each spectrum was taken using an accumulation time of 10 s and 1 accumulation was taken

The black area at the top of this map shows the area of the thinnest film, which clearly shows no enhancement. The peaks are visible as parallel lines that run the length of the map. One important feature is that the peaks do not shift in wavenumber relative to the film height. The intensity of the spectra reaches a maximum at approximately $^1/_5$ D film height, this is where the very bright spot is, on the map above. This result shows that a SERS signal is obtained from thin films and this implies that the diffraction effect is important in obtaining this enhancement.

Thick Films

The reflectance spectra for a 600 nm sample graded to ⅔ sphere height are shown in figure 3.15. The top of the sample shows the diffraction of light which leads to surface plasmon polaritons; as the film gets thicker the plasmon mode changes in wavelength and there is an interference effect when the light hits the pores, which has been discussed in more detail in Chapter one.

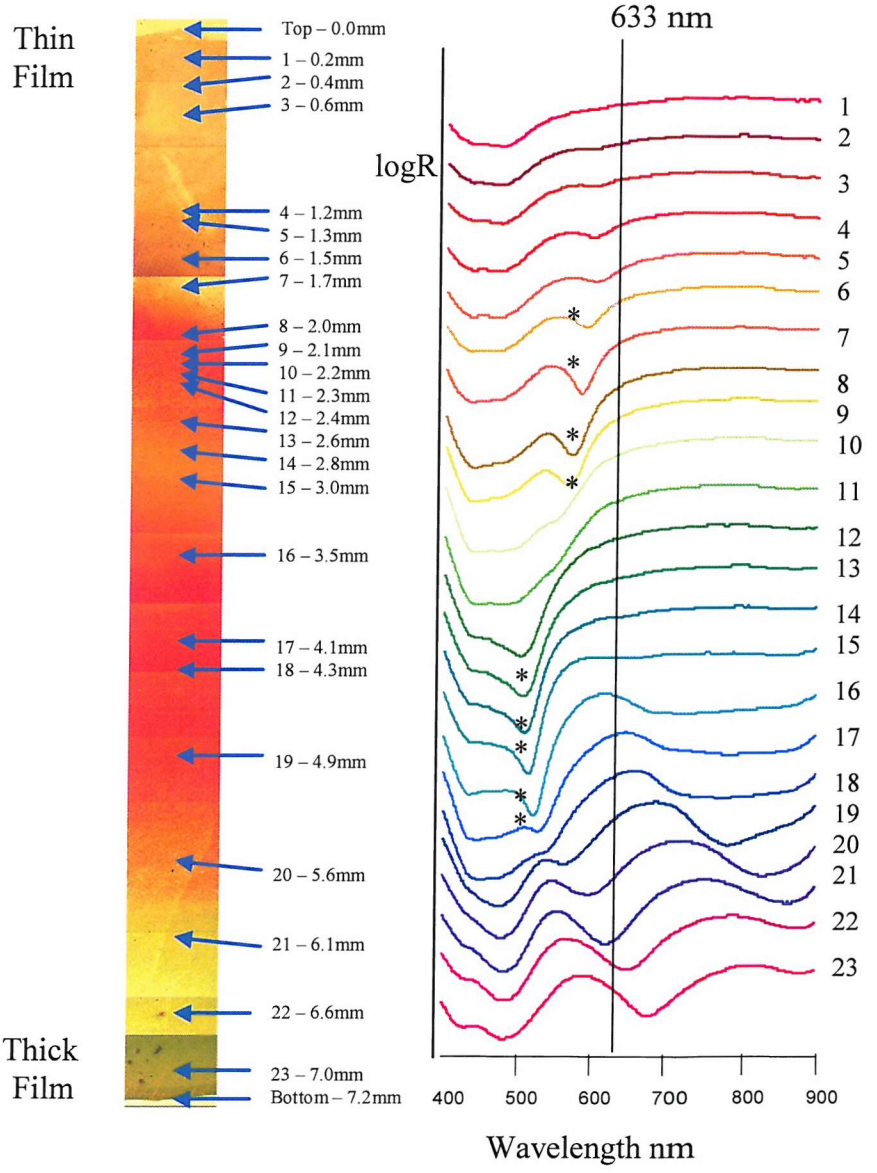

Figure 3.15: Reflectance spectra from a thick 600 nm gold nanostructure. All spectra were taken using a white light laser at 0° incidence. Spectra are plotted on a log scale and have been off set for clarity. The optical images are shown to indicate the change in colour observed, as the film height gets thicker. The blue arrows show the points from which a reflectance spectrum was taken; the distances indicate the offset from the top of the sample.

A diffraction feature at approximately 650 nm is observed in the thin film area of the sample, which agrees with the result from the thin film sample. This feature disappears around ¼ sphere height and the interference peaks are then observed which move from 500 nm to 700 nm as the film thickness increases.

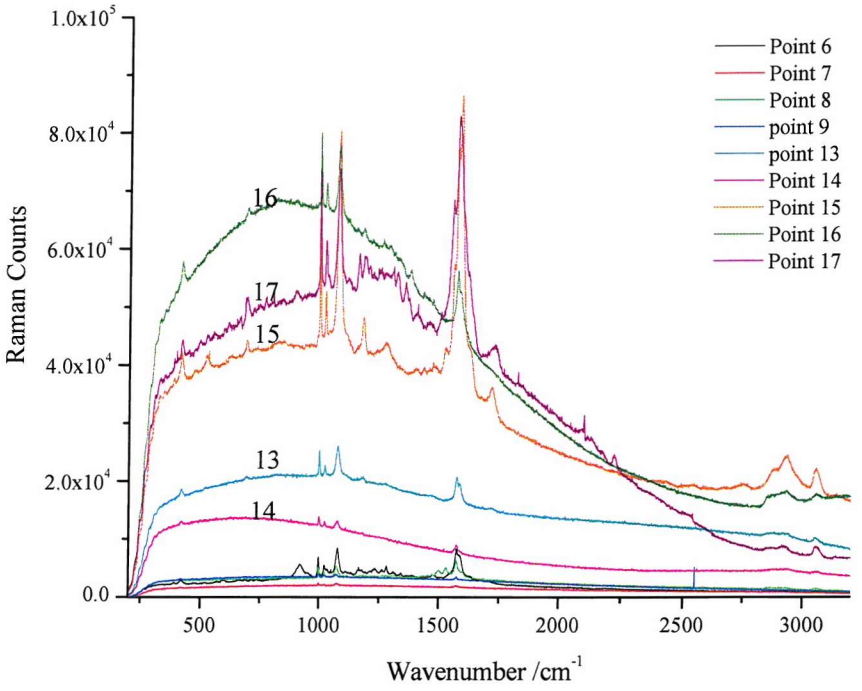

Figure 3.16: SERS spectra of benzene thiol taken from a thick film 600 nm sample, at points that showed interesting features in the reflectance spectra (shown in figure 3.13). Each spectrum was obtained using a HeNe 633 nm laser, with 1 accumulation taken at an accumulation time of 10 s.

SERS spectra of adsorbed benzene thiol were obtained from areas at which interesting features in the reflectance spectra were observed, as indicated by the * in figure 3.15, and the results are presented in figure 3.16. The spectra obtained were varied in intensity, peak heights and peak widths. Spectrum numbers 15, 16 and 17 show the most anomalous results. The spectra have a very large background, and they appear noisy. These were obtained from an area which showed large interference dips in the reflection spectra, this could imply that the interference effect also contributes to the SERS spectra, in that the reflected laser light could lead to an extra enhancement effect.

The SERS spectra obtained from the area that showed diffraction effects in the reflection spectra (Points 6-9), show a relatively weak enhancement; however the background is not

as large as for the area which was discussed previously. The results from this sample show that the areas that show an interference effect also show large backgrounds and broader peaks in the SERS spectra. Areas that showed diffraction effects in the reflection spectra showed smaller enhancements but with sharper features and a relatively smaller background.

SERS spectra were also taken every 100 μm down the sample, using the same positions on the sample as used for the reflectance spectra. The results are summarised in map form in figure 3.17.

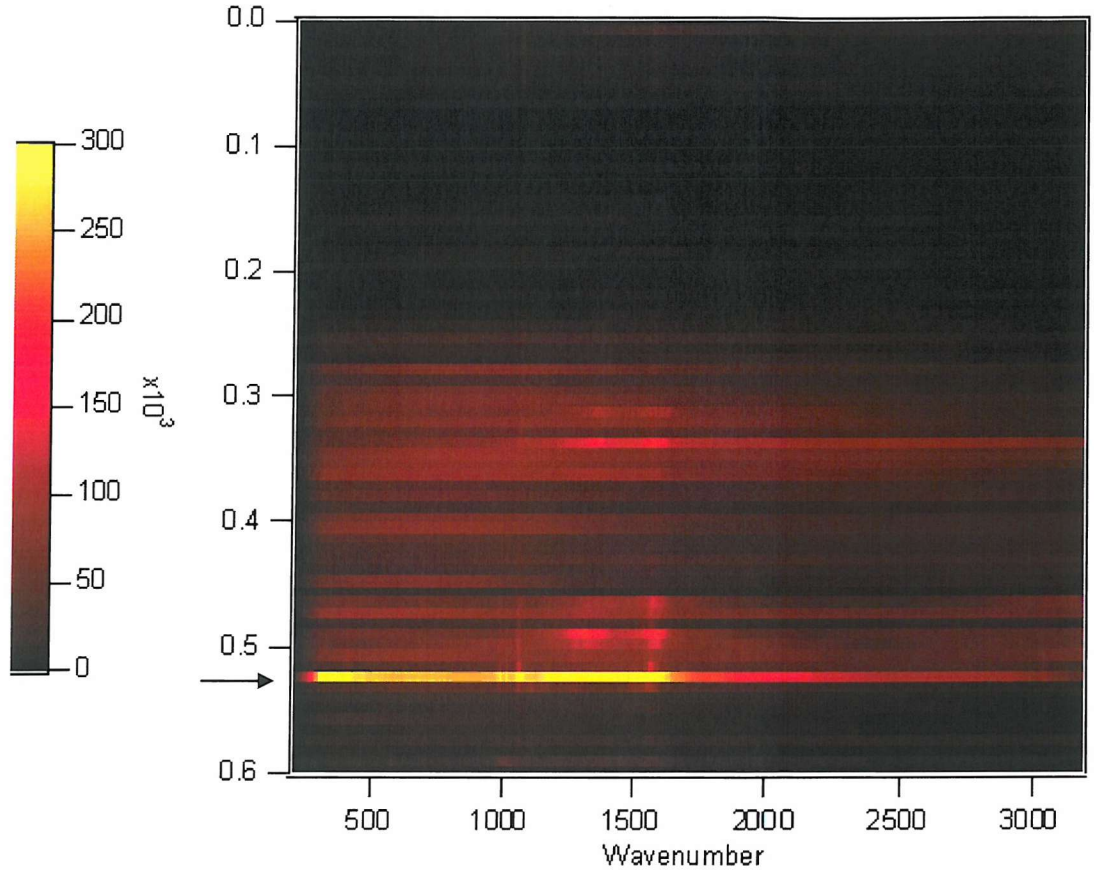

Figure 3.17: SERS spectra of benzene thiol on 600 nm gold sample with film height up to 400 nm. Spectra plotted as a function of film height/sphere size in a map form. Each spectrum was taken using an extended scan from 3200 to 200 cm^{-1} using a HeNe laser at 3 mW power. Each spectrum was taken using an accumulation time of 10 s and 1 accumulation

The results presented in the map show that there is a strong signal observed around 0.3 and 0.5 fractional sphere heights, however the background has also been enhanced to a greater extent than the thin film map showed, as the intensity scale on the map was adjusted to

provide the greatest contrast. The peaks are still visible as parallel lines down the map, and they do not shift in wavenumber. The very strong yellow band at approximately 0.52 fractional sphere height (marked with an arrow) is an anomalous spectrum which has an enormous background as well as intense peaks; this spectrum is shown in figure 3.18:

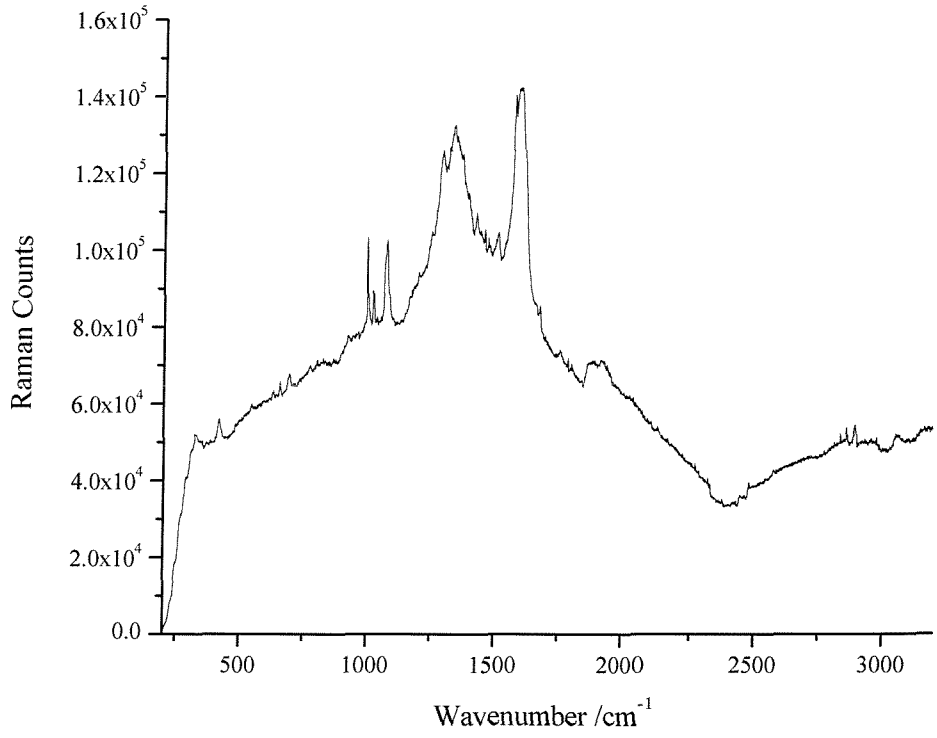

Figure 3.18: Anomalous spectrum from an area of approximately half height of a 600 nm sample. Shown as yellow band on the map in figure 3.15, indicated with an arrow.

It would appear that this is an anomalous spectrum resulting from, possibly, a structural defect or contaminant on the surface. The figure below shows the same map as above but with the colour scale changed to show the areas that are dark in the map above

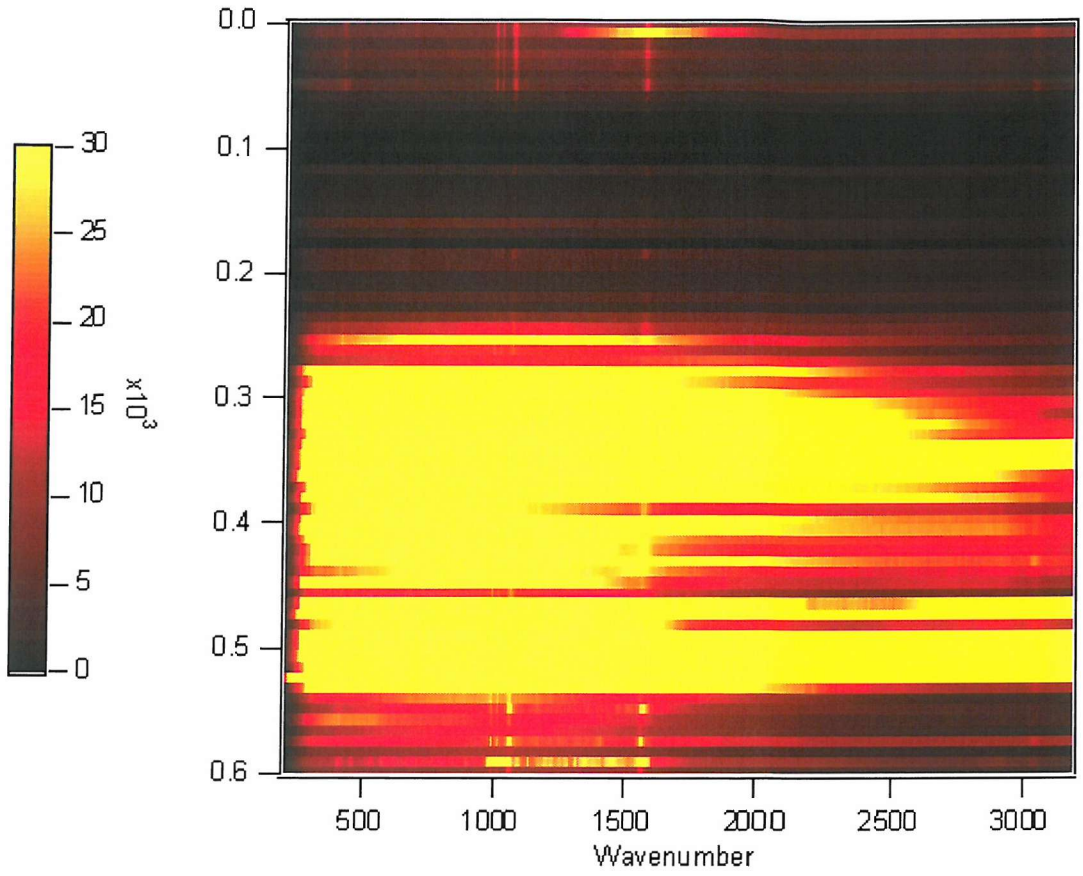

Figure 3.19: SERS spectra of benzene thiol on 600 nm gold sample with film height up to 400nm. Spectra plotted as a function of film height/sphere size as a map form. Each spectrum was taken using an extended scan from 3200 to 200 cm^{-1} using a HeNe laser at 3 mW power. Each spectrum was taken using an accumulation time of 10 s and 1 accumulation was taken

The top of the sample in the image above shows an interesting pattern similar to the map for the thin sample, shown in figure 3.14. However the enhancement is a factor of 10^2 less than the thicker film, and the original thin film sample. This could be due to a slightly different order of the template, or possibly problems with laser alignment.

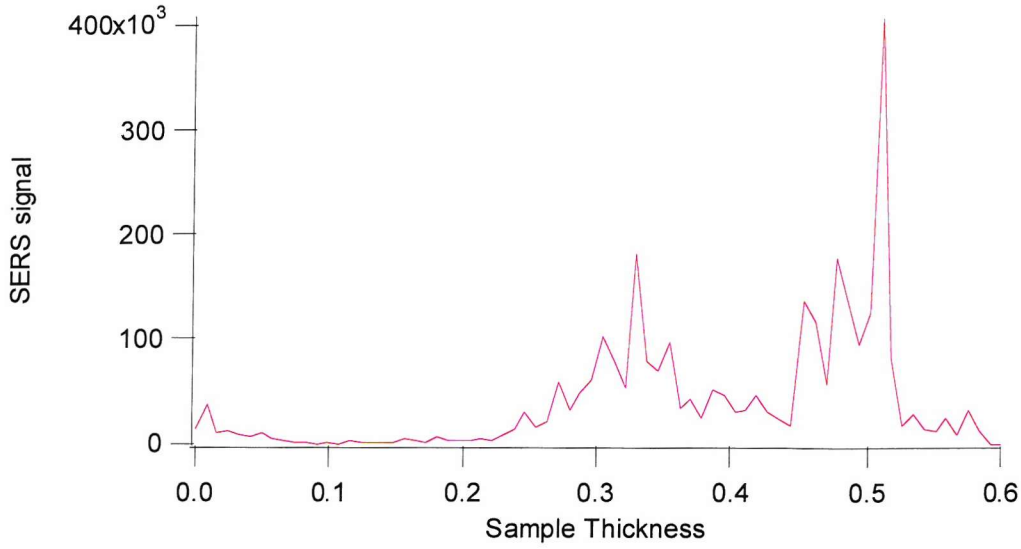

Figure 3.20: The sample thickness vs. the peak height at 1571 cm^{-1} of the SERS signal of benzene thiol on 600 nm nanostructured gold.

The effect of film thickness on the peak height of the 1571 cm^{-1} band observed in the SERS spectra of adsorbed benzene thiol is shown in figure 3.20. This graph shows that there are two strong regions of enhancement on the sample one at approximately 0.32 and the other one at approximately 0.51. In order to discover whether the enhancement is connected to the plasmon mode, SERS spectra were taken at points corresponding to the positions where the reflectance spectra were seen to change due to the plasmon modes shifting. The results are presented in figure 3.21.

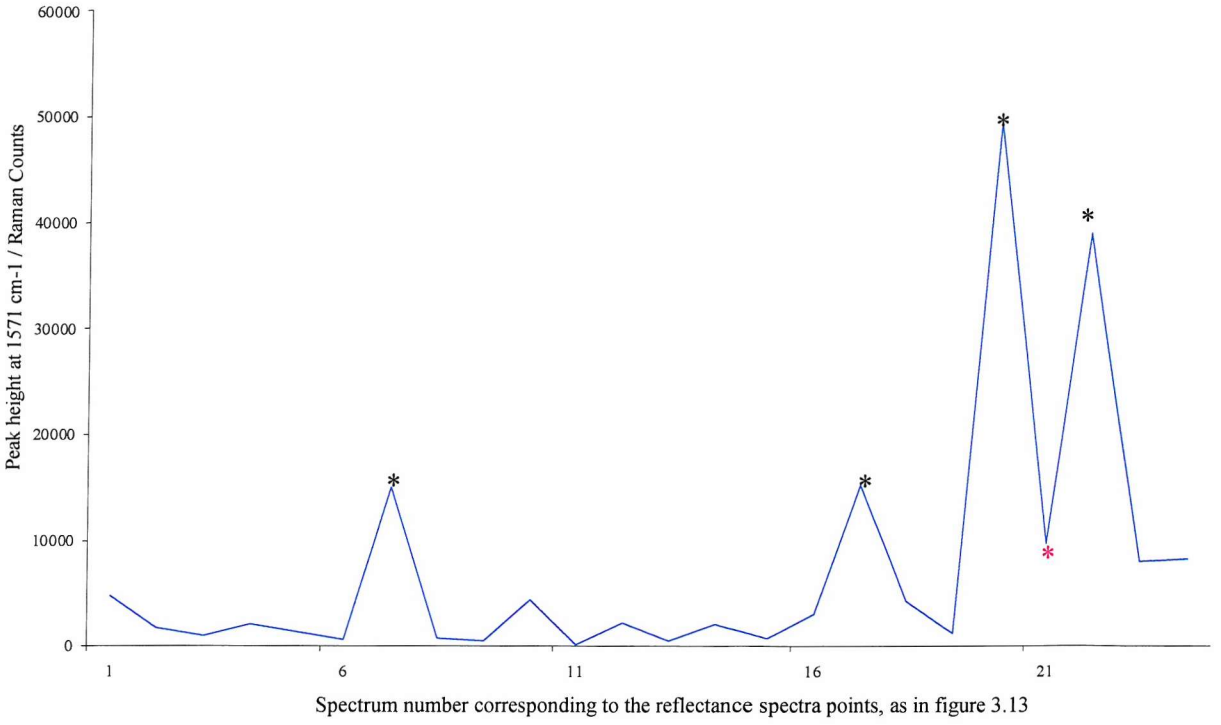

Figure 3.21: Peak height of 1571 cm^{-1} peak, at each point where a reflectance spectrum was taken.

Spectrum number 7 from this plot shows a sharp increase in peak intensity, this corresponds to reflectance spectrum number 7 which shows a very strong dip at 650 nm. Given that this is at the top (thinnest region) of the sample it would imply that this Raman signal is due to surface plasmons. The next area that shows a strong peak is spectrum number 17. The reflectance spectrum at point 17 is shows a slight interference feature at approximately 550 nm. Spectra 20 and 22 both show excellent Raman enhancements, and the corresponding reflectance spectra show a dip at approximately 630 – 650 nm. This could be either interference from the light bouncing out of the pores, or contributions from surface plasmons, as at this film height the pores would have started to close over again, (see the SEM image shown in figure 3.22). For a surface structure as shown in figure 3.22, the pore mouth diameter would be too small for the laser light to get into the pores. However the area between the voids is large enough for surface plasmons to propagate.

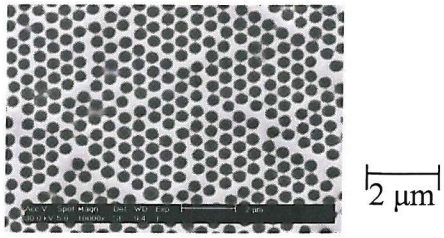

Figure 3.22: SEM image taken from the bottom of the 600 nm film where the pores had started to close over, which enables the surface plasmons to propagate around the pores.

The peak height at 21 decreases significantly in comparison to the heights at positions 20 and 22. Position 21 on the reflectance spectra shows a large dip around 633 nm, this could be due to either interference or diffraction effects. If it were interference effects, the decreased peak intensity could be due to destructive interference between the reflected Raman scattering and the incident laser light, which is at 633 nm.

3.4 Comparison of rough and nanostructured gold for Surface Enhanced Raman Spectroscopy

Roughened substrates are most commonly used for SERS, as they give the better enhancement factor when compared to other substrates. However they are very irreproducible and the surface structure is very random. Figure 3.23, below, shows SEM images of a roughened gold surface compared to a nanostructured surface, these images were collected at the same magnification.

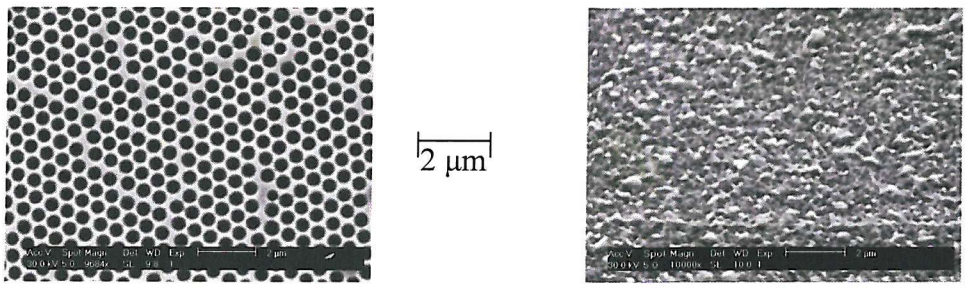

Figure 3.23: SEM images showing a 600 nm half height nanostructured film A, and an electrochemically roughened Au film B, at an angle of 30°.

The roughened gold sample was made using the procedure described by Tian *et al.* [30]. An evaporated gold substrate was placed into a solution of 0.1 M KCl, where a standard three electrode cell was used for the roughening procedure. The evaporated gold was used as the working electrode, platinum gauze was used as the counter electrode and the reference electrode was a Saturated Calomel Electrode (SCE). The potential was swept from -0.3 to 1.2 V vs. SCE, at a scan rate of 1 Vs^{-1}, the potential was then held at 1.2 V for 30 s. The potential was then swept back to -0.3 V vs. SCE at a scan rate of 0.5 Vs^{-1}, the potential was then held at -0.3 V for 1.2 s. This procedure was repeated 25 times yielding a dark brown substrate.

SERS spectra were obtained of benzene thiol adsorbed on the roughened surface. The signal from the adsorbate varied when spectra were taken from different areas of the sample. Figure 3.24 below shows three spectra of benzene thiol taken from the same roughened gold substrate. The spectra shown in figure 3.24 show that the SERS signal obtained from roughened gold varies by a factor of up to 3.5×10^4 from area to area, however the peak positions do remain consistent with each other. The irreproducibility in spectral intensity has prevented SERS from becoming a more widely used analytical technique.

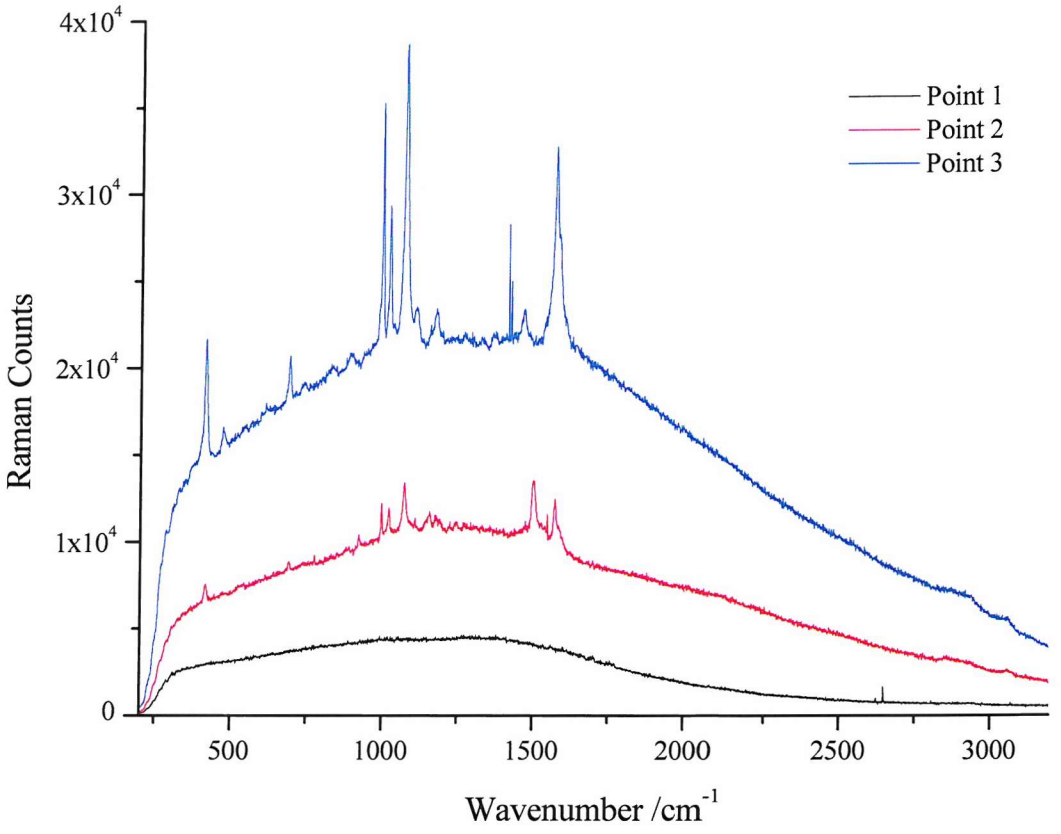

Figure 3.24: SERS spectra of benzene thiol on a roughened gold electrode. The electrode was roughened via electrochemical redox cycles in 10 mM KCl. The spectra were obtained on a 633 nm HeNe laser at 3 mW power. 1 accumulation was taken at an accumulation time of 10 s.

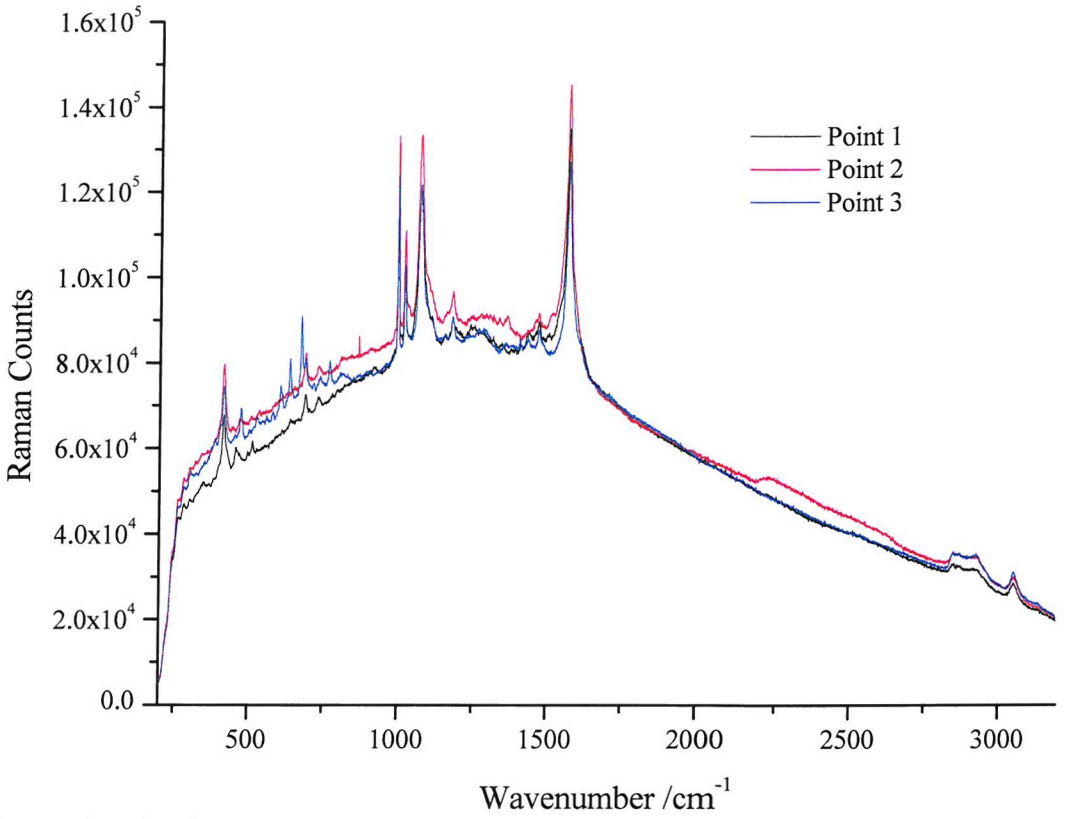

Figure 3.25: SERS spectra of benzene thiol on a nanostructured gold electrode. The sample was made from a 600 nm polystyrene sphere template, the film height is approx. 100 nm. The spectra were obtained on a 633 nm HeNe laser at 3 mW power. 1 accumulation was taken at an accumulation time of 10 s.

The spectra shown in figure 3.25, above, show three spectra taken from different positions on an area of the same film height on a 600 nm templated sample. It is clear to see that the results are reproducible for different areas. This is a very important factor for a good SERS substrate. The spectra do vary slightly in peak height and ratio of peak intensity. However the spot size of the laser is 5 μm, which could cover two domain areas of spheres (i.e. the ordering may change from hexagonal close packing to square close packing). The benzene thiol could also be held at a slightly different angle in respect to the surface, which could lead to slight differences in the bending modes of the adsorbate.

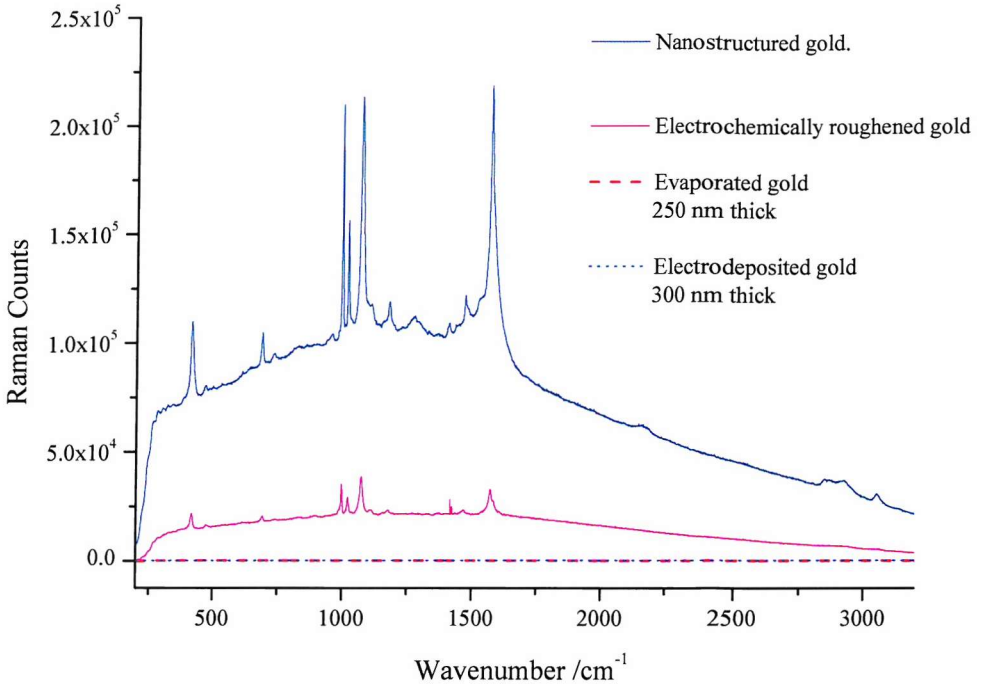

Figure 3.26: SERS spectra of benzene thiol on nanostructured, roughened, evaporated and electrodeposited gold. The nanostructured gold was based on a 600 nm template and the film height was approx. 100 nm. All spectra conditions were as previously stated.

Figure 3.26 shows a comparison between the spectra from benzene thiol on rough and nanostructured gold. The figure includes the results from evaporated and electrodeposited gold for comparison. The result shows that the nanostructured gold gave a far better signal than the roughened gold; the overall spectrum of the nanostructured gold is more intense than the rough gold by a factor of approx 10. The peaks are also more intense in comparison to the background.

3.5 Laser Wavelength Dependence

The results from this project were predominantly taken using a 633 nm HeNe laser with the Renishaw 2000 Raman system. However features are observed in the reflectance spectra between 450 and 900 nm. Thus, two other laser wavelengths were tested on the thin film 600 nm sample that was analysed previously in this project to investigate the relative contributions of the phenomena that produce the diffraction and interference features in the reflectance spectra to the SERS enhancement.

The benzene thiol was stripped from the surface, used previously for the studies at 633 nm laser excitation, electrochemically using the cyclic voltammetry method discussed in section 3.2. The sample was then cleaned in Tetra Hydrofuran (THF) for 24 hours, to ensure that there were no contaminants left on the surface. A fresh layer of 5 mM benzene thiol was then assembled onto the surface and the SERS spectrum was taken using a 785 nm diode laser and a 514 nm Ar^+ laser.

The same position on the sample was analysed for each laser. This was chosen as the area that gave the best signal on the HeNe 633 nm laser, from the map shown in figure 3.12. An image of the bottom corner of the sample was taken using the optical camera attached to the microscope, then the sample was moved in the x and y direction, using the stage, to the same point for each laser. A reflection spectrum was also obtained from this point, which is shown in figure 3.27.

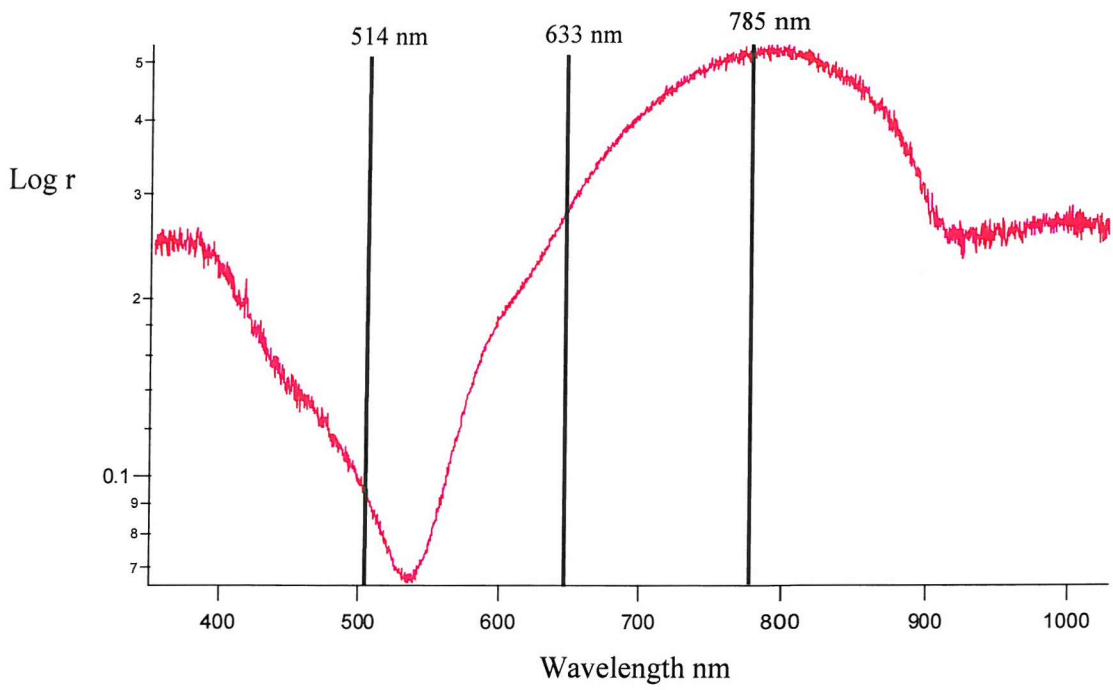

Figure 3.27: Reflection spectrum obtained from a thin film 600 nm templated sample, at the point where SERS spectra were obtained for 514 nm, 633 nm and 785 nm laser excitations

The spectrum shows a dip in reflectivity at 550 nm and a broad peak at 800 nm. From previous correlation studies between the SERS spectra and reflection spectra a prediction can be made that the 514 nm and 633 nm laser wavelengths should show a greater

enhancement at this particular point on the sample. The resulting spectra of benzene thiol for each laser wavelength is shown in figure 3.28.

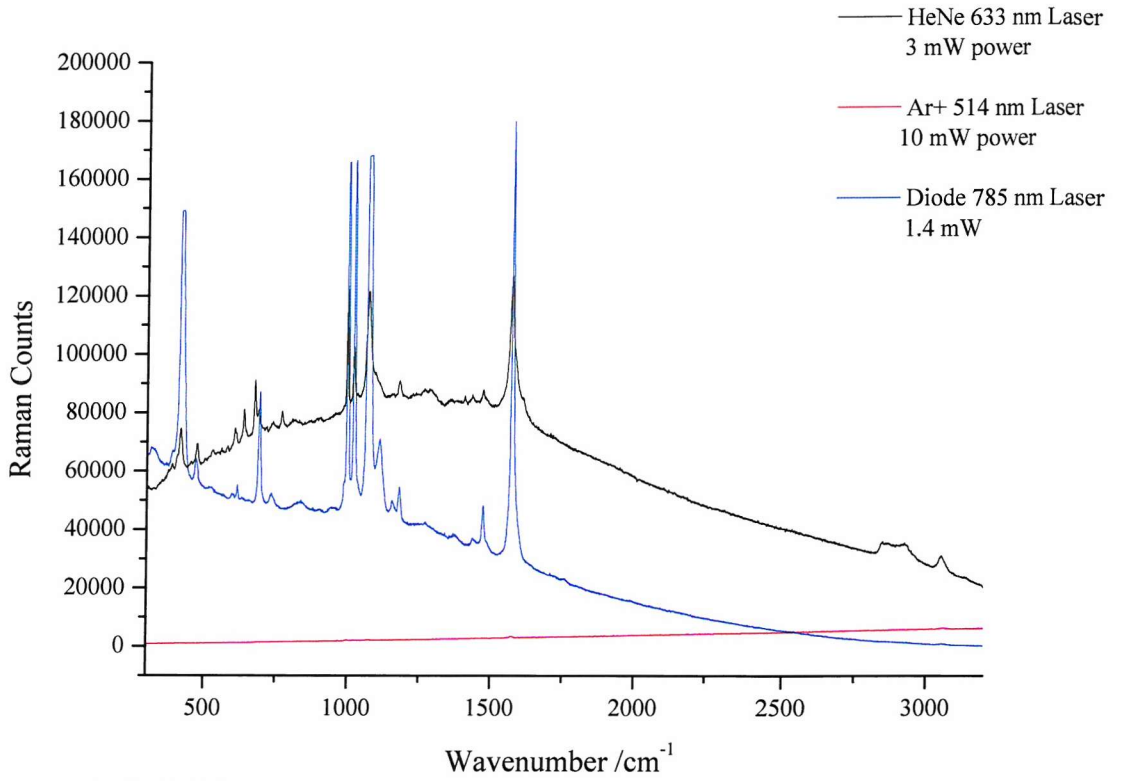

Figure 3.28: SERS spectra taken from an area of thin film of a 600 nm sample. The spectra were taken from a 785 nm diode laser, a 514 nm Ar^+ laser and a 633 nm HeNe laser. The power of each laser is shown in the figure legend. Each spectrum was recorded using an extended scan range from 3200 to 200 cm^{-1}, with an accumulation time of 10 s. 1 accumulation was taken.

Figure 3.28, shows the comparison between spectra taken from different lasers using a thin film 600 nm sample. The main feature from this figure is the differences in the shape of the background observed from each wavelength laser. The 633 nm laser shows a very broad background that appears to peak around 1500 to 1000 wavenumbers, this is most likely due to a fluorescence effect. The spectrum from the 785 nm laser shows an increase in background as the spectrum tends toward low wavenumbers. The ratio in peak heights also appears to be different for the 785 nm laser in comparison to the 633 nm laser. However, the thiol was stripped and the substrate cleaned, after the spectra were obtained with the 633 nm laser. The thiol was then reassembled onto the surface before the spectra were

obtained from the 785 nm laser. The thiol could therefore be arranged differently on the surface which would yield different peak ratios.

It should be noted that different laser powers were used for the different lasers. The results from the 785 nm laser were taken at approximately half the power (mW) of the results from the 633 nm laser. When a spectrum was taken using the same power the spectra were so intense that they saturated the detector.

The results presented for the laser wavelength dependence study are still under investigation. The excellent result from the 785 nm diode laser was unexpected as there are no features in the reflectance spectrum for this sample at this wavelength. The reflectance spectrum was obtained approximately 10 weeks after the laser dependence study; therefore the sample may have degraded over time.

3.5.1 Power Dependence

There is clearly a relationship between the laser power and the spectral intensity. The 785 diode laser was used at varying powers to establish the relationship. The peak height at 693 cm^{-1} was then traced at each power. The results are shown in figure3.29:

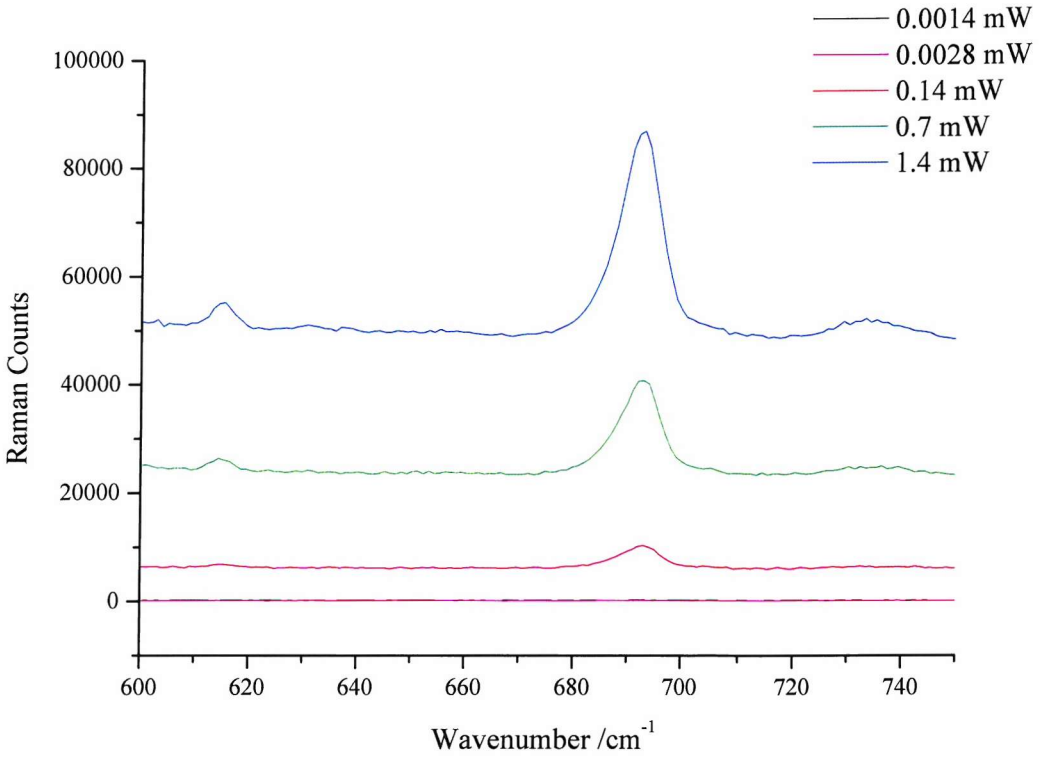

Figure 3.29: Enlarged image of the peak at 693 cm^{-1} at varying powers of a 785 nm diode laser. The powers are shown above in the figure legend. Each spectrum was obtained using an extended scan range from 3200 cm^{-1} to 200 cm^{-1}. The scan time was 10 s, and 1 accumulation was taken.

The different spectra clearly show that the peak intensity increases with power. For clarity the laser power has been plotted vs. peak height at 693 cm^{-1}, shown in figure 3.30.

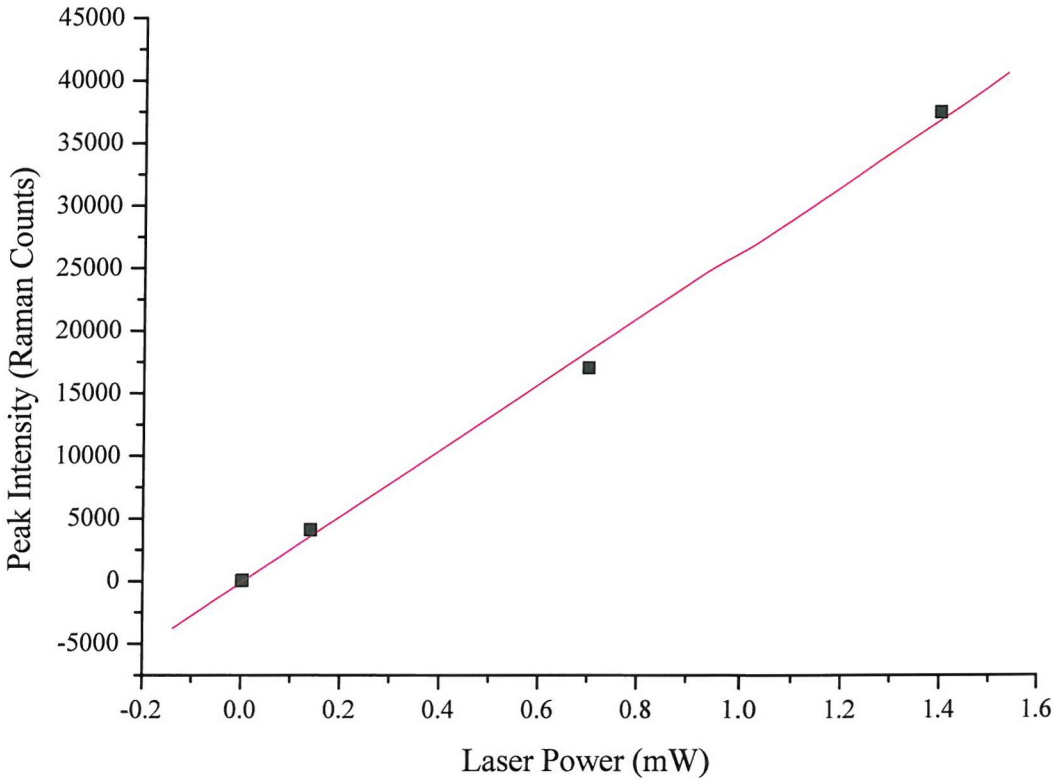

Figure 3.30: Laser power vs. peak height at 693 cm^{-1}. Spectra were obtained using 785 nm diode laser at various powers, indicated in figure 3.30.

Figure 3.30 shows that the spectra increase linearly with laser power.

The main observations from the laser dependence study show that:

1. The laser wavelength changes the shape of the background of the spectrum.
2. The 785 nm laser appears to give the best signal to background ratio for a 600 nm sample.
3. The 514 nm laser produced very little signal from the benzene thiol.

This would imply that different sphere sizes could be tried at different wavelengths to produce excellent SERS for any sphere size.

3.6 SERS on Nickel nanostructures.

The results presented in sections 3.3 through 3.5 have undoubtedly shown that gold nanostructures prepared by templated deposition do produce excellent SERS spectra, which are reproducible. However gold is a very common metal for use in SERS, therefore if the same result could be reproduced for a metal that is not commonly used in Raman spectroscopy, it would help to show that the structure is producing the enhancement and not the metal.

Nickel is not a common metal used for SERS. However, recently Tian *et al.*[31] have used it for *in-situ* electrochemical SERS of pyridine in solution. Nanostructured Ni surfaces were prepared by templated electrodeposition through arrays of 600 nm spheres from a solution of 0.1 M $NiSO_6$, 0.1 M H_3BO_3 and 5 mM SDS which was adjusted to pH 3.2 using H_2SO_4. The structured films were cleaned by immersion in THF, as discussed previously for the gold nanostructured surfaces. The samples were then soaked a 10 mmol dm-3 aqueous solution of pyridine and the SERS spectra were collected using 633 nm laser excitation.

The spectrum obtained, however showed no peaks at all for pyridine, we presume that the nickel did not adsorb the pyridine without the electrochemical charge that would be passed through the electrode in *in-situ* electrochemical SERS.

Benzene thiol was adsorbed onto the surface, to aid comparison to all other results presented in this project; the spectrum obtained is shown in figure 3.31. Very little Raman signal from the adsorbed benzene thiol was observed, with a very low signal to noise ratio.

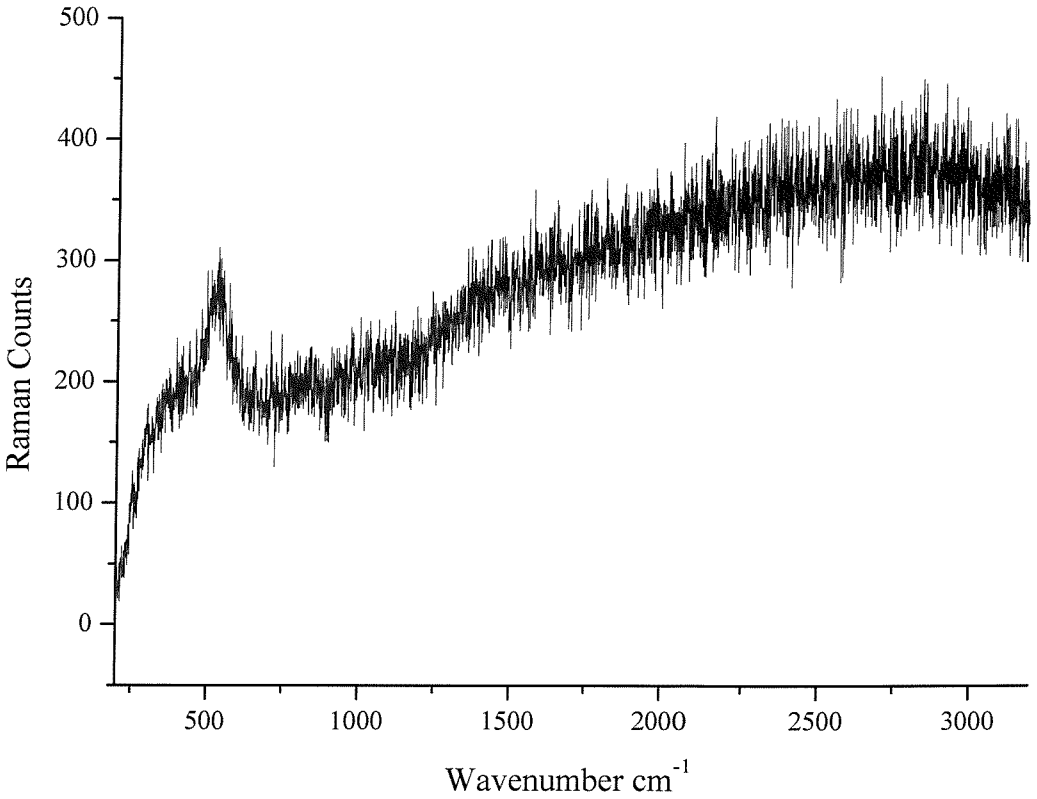

Figure 3.31: SERS spectrum of benzene thiol on a nanostructured nickel sample, with 600 nm pores.

3.6.1 Gold topped nickel 600 nm cavities.

The lack of SERS signal from the Ni surface enables this surface to be used in conjunction with the Au surface to separate the contributions to the SERS enhancement from the surface plasmons and the interference effects. By making a structure that consists of nickel cavities with a gold surface, only the signal observed from the gold surface plasmons should contribute to the SERS. Alternatively a structure that consisted of gold cavities with a nickel top, should produce SERS from the confined plasmons within the cavity i.e. the interference effect.

A gold topped nickel layered structure was made by the usual templating method discussed in Chapter two using 600 nm spheres. The nickel film was graded up to approximately ¾

sphere height. A 50 nm layer of gold was then plated on top of the structure. The deposition potential for gold onto nickel was found to be -0.75 V vs. SCE.

The sample was a 600 nm template and the film was graded up to 500 nm film height with 5 steps with step widths of 100 nm. The gold layer was then plated on top of the nickel. When the spheres were removed a structure that consisted of nickel cavities and gold tops was obtained, as shown in figure 3.32:

Figure 3.32: Schematic diagram showing gold topped nickel cavity

Theoretically, the nickel cavity should not yield any SERS signal as the spectrum shown in figure 3.31, which is that of a pure nickel substrate, did not show a benzene thiol signal.

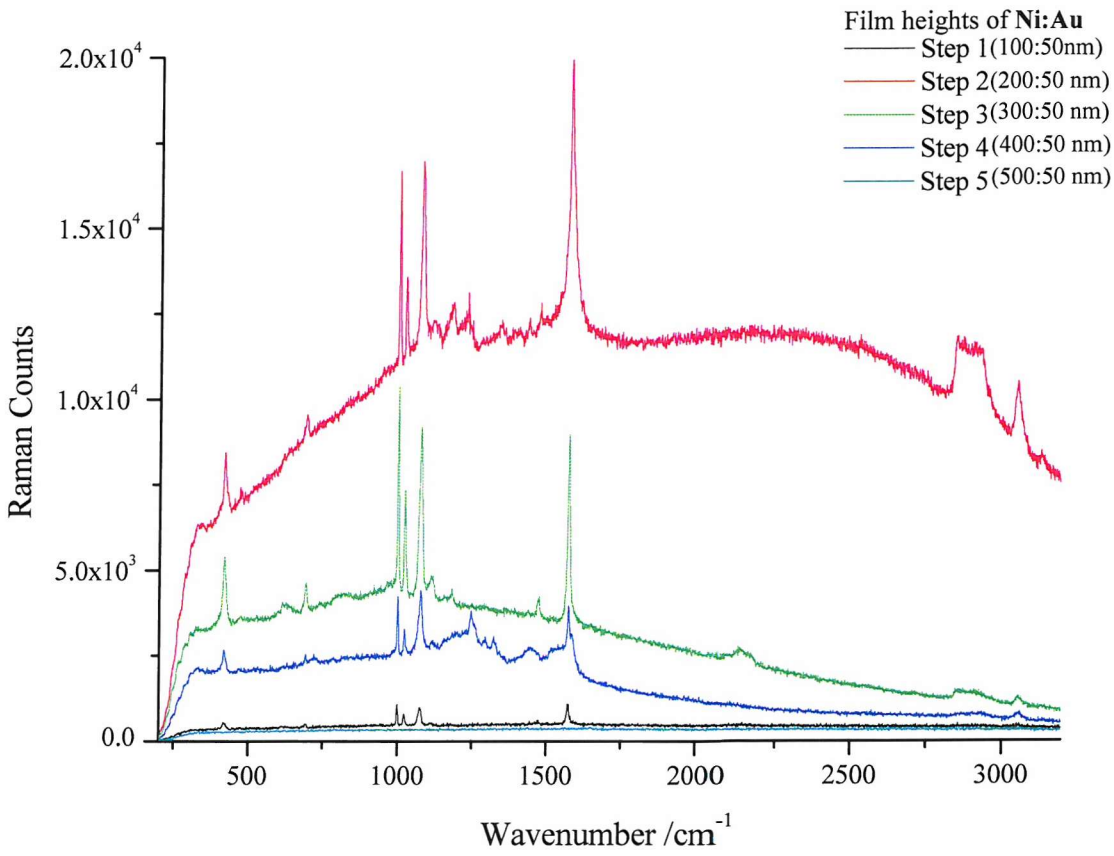

Figure 3.33: SERS spectra taken from each step of the gold topped nickel cavities. The spectra were obtained using the same conditions that have previously been stated.

Figure 3.33 shows that the SERS signal observed changes for each step of the sample. The first step, which is 100 nm Ni covered with 50 nm Au, shows a relatively small enhancement. The enhancement increases at the second step, however the background also increases dramatically giving an anomalous spectrum. The third step is at approximately half sphere height and the signal observed shows very sharp, well defined peaks. The signal to background ratio also seems to have decreased. The final steps show a marked decrease in signal. When the cavities start to close over the reflection spectra of the nanostructures show a interference effect, which arises from the localised plasmons within the cavity. The results above would imply confined plasmons in the nickel cavities do not give rise to SERS signals, and the enhancement observed in a result of the surface plasmons.

3.6.2 Nickel topped gold 600 nm cavities.

The same preparation procedure for this sample was followed as for the gold topped nickel sample. The sample was based on the 600 nm sphere diameter template, and the sample had 9 steps each with a step width of 50 nm leading to an overall film height of 450 nm of gold. The sample was then topped with 50 nm of nickel, giving the sample a blue/silver colour.

Figure 3.34: Schematic diagram showing a nickel topped gold cavity

Spectra were taken at each step of the sample, the results are shown below:

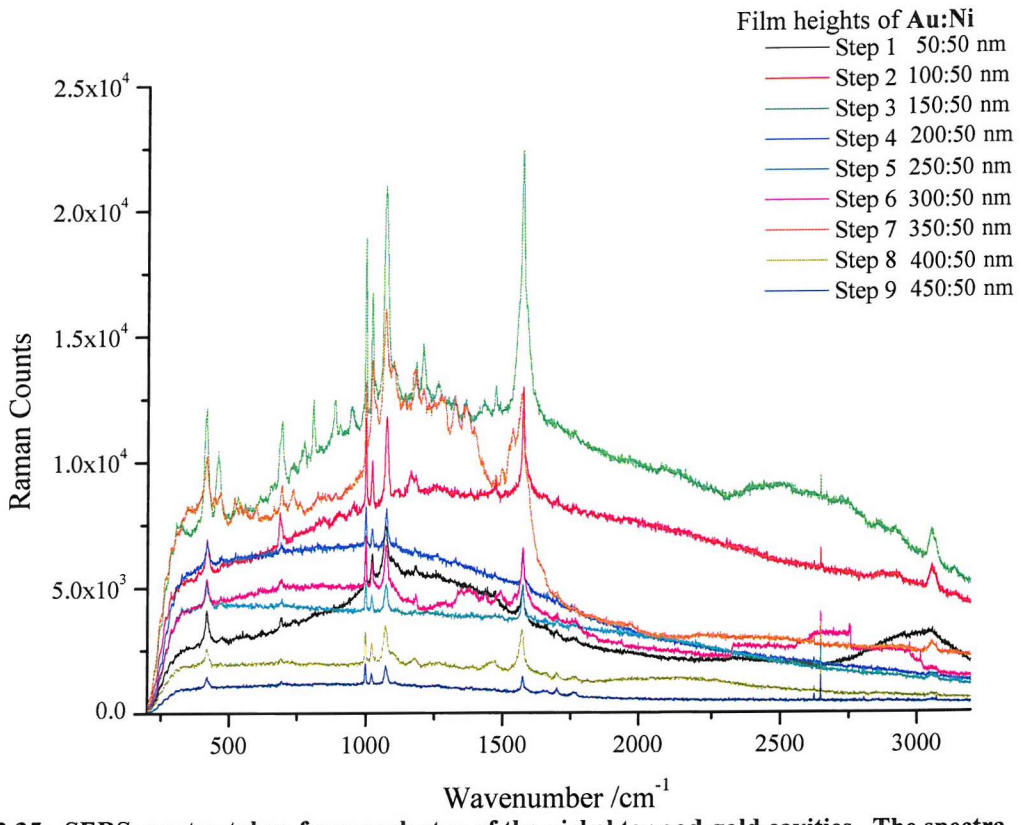

Figure 3.35: SERS spectra taken from each step of the nickel topped gold cavities. The spectra were obtained using the same conditions that have previously been stated.

The spectra shown in figure 3.35 show a general increase in spectral intensity until step 3 (150 nm gold 50 nm nickel). The next steps show a decrease in signal, except for step 7 shown in figure 3.36, which was anomalous and has been attributed to contaminants at this point of the sample.

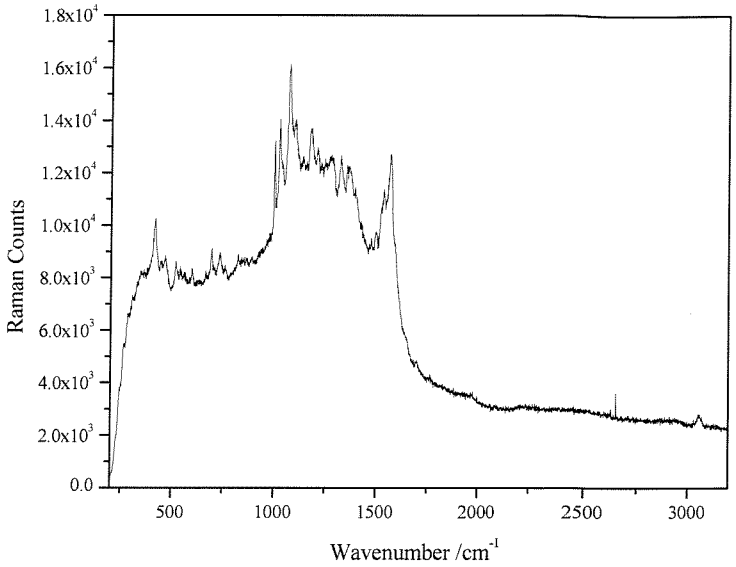

Figure 3.36: SERS spectrum of benzene thiol from step 7 of nickel topped gold cavity structure, the spectrum is shown individually for clarity.

In general the results from the nickel topped gold cavities are consistent with the inverse structure, which implies that the enhancement observed for all gold structures arises from a combination of surface and confined plasmons. The enhancements are approximately the same as for all gold structures.

Chapter Four: Conclusions

The main conclusion made from this project is that SERS can be obtained from nanostructured gold structures, and the enhancement factor was more than for a roughened gold electrode. The spectra are also reproducible for different areas of sample, from sample to sample, whereas SERS spectra from roughened gold electrodes vary from position to position.

The sphere size of the gold template, which produced the best SERS signal, was 600 nm. This showed good enhancement at thin film, and also film around half sphere height. This would imply that the enhancement comes from both surface and confined plasmons. The results from the nickel/gold samples showed that there was enhancement obtained from both the samples. It was shown that a pure nickel sample did not show any signal, therefore the SERS obtained from the nickel/gold samples must have come from the gold in the sample, either on the surface or from within the cavities. The strongest signal from this experiment came from the surface plasmons found at thin films, where there is a large enough area between the spheres for the plasmon to propagate.

The idea of the surface plasmons corresponds well with original results from roughened surfaces, and recent results from Tessier[8], Van Duyne[32] and Vo-Dinh[7] that show good SERS signals from metal colloid structures and metal nano-structured spheres respectively.

It was also found that laser wavelength affected the SERS spectrum obtained. In this project the best wavelength for a 600 nm structure was 785 nm, and 514 nm had a very low signal to noise ratio, which led to very little signal being observed. This implies that different sphere sizes may show good SERS signals from different wavelength lasers. There was also a linear relationship found to exist between the laser power and peak height.

The nanostructured gold films studied in this project show excellent SERS spectra, they also look very promising in terms of being able to tune different laser wavelengths to sphere sizes to give the best possible signal.

Chapter Five: Future Work

The results obtained from this project have sparked so many other ideas that there was not enough time to complete them all in one year.

The results obtained from the laser wavelength dependence study, imply that different laser wavelengths could be used with different sphere sizes to give good SERS signals. To test this each different sphere size would be tested with all three different lasers used in this project to investigate whether there was any correlation between the two variables.

Gold nanostructures were used predominantly in this project. However silver was originally used in Fleischmann's experiments, and it is the most commonly used metal for SERS. Silver readily oxides with air and therefore it is a problem for a SERS substrate that is not used *in-situ*, such as the substrate in this project. Some work has been done on producing silver nanostructures and the original results seem to suggest that silver nanostructures could produce better SERS spectra than gold. Copper and platinum would also be very promising metals to try as they are very stable metals.

As stated previously the enhancement seen in this project looked like it came from a combination of surface and confined plasmons. With the surface plasmons being more influential than the confined plasmons. Therefore, the inverse structure to that used in this project would theoretically be an excellent substrate. The spheres would all be regularly aligned and of the same size, which would again be variable by using different sphere sizes for the original template.

The inverse structure is obtainable by plating around the spheres using an insulating material such as a polymer. The spheres can then be dissolved in the usual manner leaving the polymer structure. There is a small area of gold at the bottom of each polymer dish that would still be conducting, which arises from the point where the sphere touched the gold substrate. Gold can be plated into each cavity using the technique described in this projecr,

through the connection at the bottom of the dish. The polymer can then be dissolved or burnt away leaving the metal spheres.

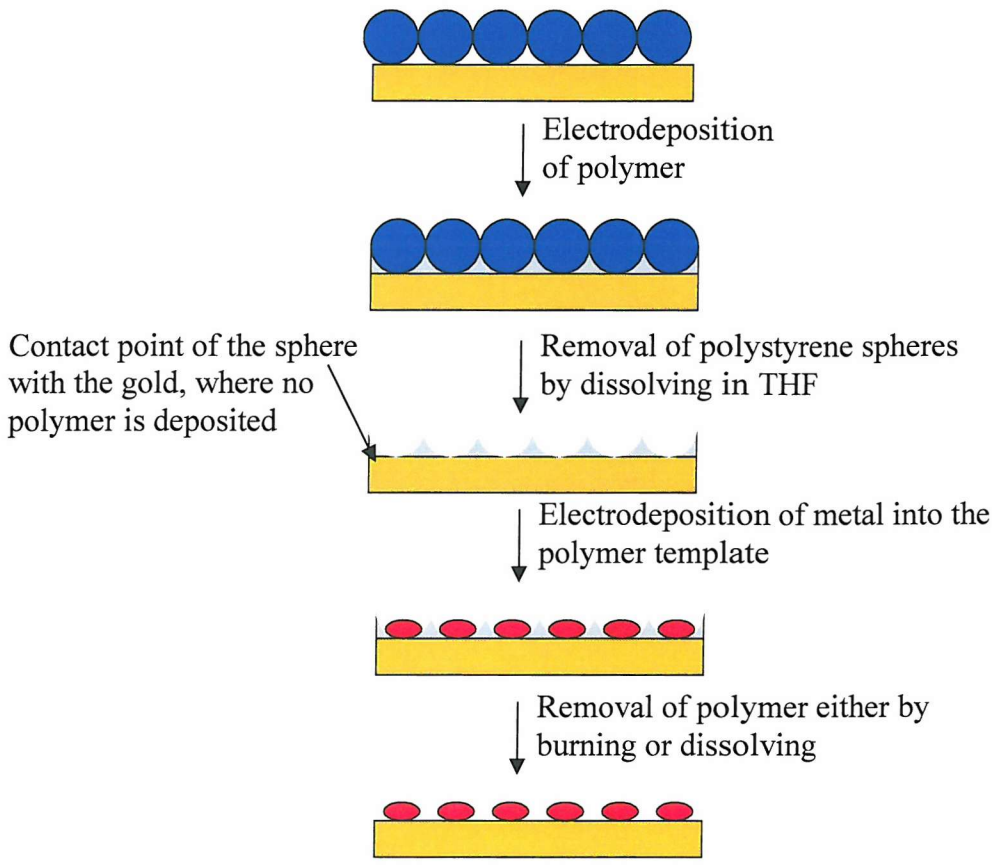

Figure 4.01: Schematic diagram showing the double templated method to yield nanodot structures

The technique is known as the double template method, and the structure obtained could make an ideal SERS structure, given that the surface area would be increased and the spheres would still be in a highly ordered array.

Chapter Six: References

1. Fleischmann, M., P.J. Hendra, and A.J. McQuillan, Chem. Phys. Lett., 1974. **26**(2): p. 163-166.
2. Raman, C.V. and K.S. Krishnan, Indian J. Phys, 1928. **2**: p. 387.
3. Jeanmaire, D.L. and R.P. Van Duyne, J. Electroanal. Chem. Interfacial Electrochem, 1977. **84**(1): p. 1-20.
4. Albrecht, A. and C.G. Creighton, J. Am. Chem. Soc., 1977. **99**: p. 5215 - 5217.
5. Kambhampati, P., et al., Journal of chemical physics, 1998. **108**(12): p. 5013 - 5026.
6. Kim, N.H. and K. Kim, Chem. Phys. Let, 2004. **393**: p. 478-482.
7. Vo-Dinh, T., Tr. Anal. Chem., 1998. **17**(8-9): p. 557-582.
8. Tessier, P.M., et al., J. Am. Chem. Soc., 2000. **122**(39): p. 9554-9555.
9. King, F.W., R.P. Van Duyne, and G.C. Schatz, J.Chem. Phys., 1978. **69**(10): p. 4472.
10. Webber, W.H. and G.W. Ford, Phys. Rev. Lett, 1980. **44**: p. 1774.
11. Webber, W.H. and G.W. Ford, Surf. Sci., 1981. **109**(2): p. 451.
12. Moskovits, M., Rev. .Mod. Phys., 1985. **57**(3): p. 783-826.
13. Aizpurua, J., et al., Phys. Rev. Lett., 2003. **90**(5): p. 057401-1 - 057401-4.
14. Bartlett, P.N., et al., Faraday, 2004. **125**: p. 117 - 132.
15. Hao, E., et al., J. Phys. Chem. B, 2004. **108**: p. 1224 - 1229.
16. Imhof, A. and D.J. Pine, Nature, 1997. **389**(6654): p. 948-951.
17. Velev, O.D., et al., Nature, 1999. **401**: p. 548.
18. Braun, P.V. and P. Wiltzius, Nature, 1999. **402**: p. 603-604.
19. Sanchez - Gil, J.A. and J.V. Garcia - Ramos, Chem. Phys. Lett., 2003. **367**: p. 361-366.
20. Palacios-Lidon, E., et al., Adv. Mater., 2004. **16**(4): p. 341 - 345.
21. Liu, F.K., et al., Microelectr. Eng., 2003. **67-8**: p. 702-709.
22. He, H.X., et al., Langmuir, 2000. **16**(8): p. 3846 - 3851.
23. Dimitrov, A.S. and K. Nagayama, Langmuir, 1996. **12**(5): p. 1303-1311.
24. Dimitrov, A.S., et al., Langmuir, 1994. **10**(2): p. 432-440.
25. Kralchevsky, P.A. and N.D. Denkov, Current Opinion in Colloid & Interface Science, 2001. **6**: p. 383-401.
26. Baryshev, A.V., et al., Physica E, 2003. **17**: p. 426-428.
27. Rand, D.A.J. and R. Woods, J. Electroanal. Chem. Interfacial Electrochem, 1971. **31**(1): p. 29-38.
28. Trasatti, S. and O.A. Patril, Pure Appl. Chem., 1991. **63**(5): p. 711-734.
29. Han, S.W. and K. Kim, J.Colloid and Interface Science, 2001. **240**: p. 492 - 497.
30. Tian, Z.Q., B. Ren, and D.Y. Wu, J. Phys. Chem. B, 2002. **106**(37): p. 9463-9483.
31. Huang, Q.J., et al., J. Electroanal. Chem., 2004. **563**: p. 121 - 131.
32. Haynes, C.L. and R.P. Van Duyne, J. Phys. Chem. B, 2003. **107**: p. 7426 -7433.